

Cognitive Neuropsychology

ISSN: 0264-3294 (Print) 1464-0627 (Online) Journal homepage: www.tandfonline.com/journals/pcgn20

A case study of early-emerging prosopometamorphopsia

Sydney Fortner, Antônio Mello, Daniel Stehr, Chandana Kodiweera, Heejung Jung, Sarah Kerns, Krzysztof Bujarski, Tor Wager & Brad Duchaine

To cite this article: Sydney Fortner, Antônio Mello, Daniel Stehr, Chandana Kodiweera, Heejung Jung, Sarah Kerns, Krzysztof Bujarski, Tor Wager & Brad Duchaine (30 Oct 2026): A case study of early-emerging prosopometamorphopsia, Cognitive Neuropsychology, DOI: 10.1080/02643294.2026.2755076

To link to this article: https://doi.org/10.1080/02643294.2026.2755076

© 2026 The Author(s). Published by Informa UK Limited, trading as Taylor & Francis Group

View supplementary material

Published online: 30 Oct 2026.

Submit your article to this journal

Article views: 77

View related articles

View Crossmark data

Full Terms & Conditions of access and use can be found at https://www.tandfonline.com/action/journalInformation?journalCode=pcgn20

COGNITIVE NEUROPSYCHOLOGY
https://doi.org/10.1080/02643294.2026.2755076

Routledge
Taylor & Francis Group

OPEN ACCESS Check for updates

A case study of early-emerging prosopometamorphopsia

Sydney Fortner [a,b], Antônio Mello [a], Daniel Stehr [a], Chandana Kodiweera [a], Heejung Jung [c], Sarah Kerns [a], Krzysztof Bujarski [d], Tor Wager [a] and Brad Duchaine [a]

[a]Department of Psychological and Brain Sciences, Dartmouth College, Hanover, NH, 03755, USA; [b]Department of Psychological and Brain Sciences, UCSB, Santa Barbara, CA, 93109, USA; [c]Department of Neurology and Neurological Sciences, Stanford Medical School, Stanford, CA, 94305, USA; [d]Department of Neurology, Dartmouth-Hitchcock Medical Center, Lebanon, NH, 03784, USA

ABSTRACT

Prosopometamorphopsia (PMO) is a rare perceptual disorder characterized by facial distortions. This report presents the first thorough study of early-emerging PMO. Zed, who was 15 years old when first tested, has experienced lifelong, dynamic facial distortions in which features move, droop, disappear, expand, and rotate. He also experiences identity misrecognitions, perceiving familiar faces as strangers and vice versa. Behavioural assessments indicate Zed's distortions persist across different viewpoints, visual field positions, picture-plane orientations, and visual angles. Neuropsychological testing revealed deficits in face identity recognition, yet Zed performed normally on tests requiring fine-grained perception of facial age and sex. While structural MRI showed no lesions, MRI revealed reduced face-selectivity in right posterior face-selective areas, and diffusion tensor imaging indicated lower white matter integrity in the left inferior fronto-occipital fasciculus. This case offers novel insights into the manifestations of early-emerging PMO, its co-occurrence with other face-processing disorders, and its underlying neural correlates.

ARTICLE HISTORY
Received 17 February 2026
Revised 30 July 2026
Accepted 4 October 2026

KEYWORDS
Prosopometamorphopsia; face perception; developmental Prosopagnosia; occipital face area; fusiform face area; inferior fronto-occipital fasciculus

1. Introduction

Prosopometamorphopsia (PMO) is a rare visual disorder characterized by distortions in facial appearance, including alterations in shape, texture, feature positioning, and color. These distortions can affect both sides of the face (bilateral PMO) or just one side (hemi-PMO). In some cases, facial distortions are dynamic, while in others, they remain stable over time (Blom et al., 2021; Herald et al., 2023).

The first documented case of PMO was published in 1904 when Lachmund described a 37-year-old woman, W., who, following three consecutive epileptic seizures, perceived her eyes as enlarged and "contorted", with her head expanding when looking in the mirror (Lachmund, 1904). The term "prosopometamorphopsia" was introduced decades later by MacDonald Critchley (Critchley, 1953), who coined the term by combining the Greek prosopon ("face") with metamorphopsia (the medical term for visual distortion). Since Lachmund's report, fewer than 100 PMO cases have been documented (Blom et al., 2021; Herald et al., 2023). Nearly all reports involve individuals who acquired PMO later in life, after years of typical face perception. Common causes of acquired PMO include severe head trauma, epilepsy, brain tumors, stroke, and multiple sclerosis (Blom et al., 2021). Lesions within the face-processing network (specifically the occipital face area and fusiform face area) and the splenium of the corpus callosum are commonly observed in acquired PMO (Blom et al., 2021; Herald et al., 2023), and intracranial stimulation of posterior face-selective brain regions can induce distortions resembling PMO symptoms (Jonas & Rossion, 2021; Parvizi et al., 2012; Puce et al., 1999; Rangarajan et al., 2014).

In many neuropsychological conditions, however, a substantial proportion of affected individuals exhibit no clear history of brain lesions and are instead classified as having a developmental disorder (Castaldi et al., 2020; Mello & Duchaine, 2025; Peterson & Pennington, 2015). To date, only one reported PMO case appears developmental in origin. The one-page case study described a 52-year-old woman who reported lifelong facial distortions, often perceiving faces as "dragon-like." After prolonged viewing (i.e., several minutes), faces "turned

CONTACT Sydney Fortner sydneyfortner@ucsb.edu
Supplemental data for this article can be accessed online at https://doi.org/10.1080/02643294.2026.2755076.

© 2026 The Author(s). Published by Informa UK Limited, trading as Taylor & Francis Group
This is an Open Access article distributed under the terms of the Creative Commons Attribution License (http://creativecommons.org/licenses/by/4.0/), which permits unrestricted use, distribution, and reproduction in any medium, provided the original work is properly cited. The terms on which this article has been published allow the posting of the Accepted Manuscript in a repository by the author(s) or with their consent.

black, grew long, pointy ears and a protruding snout, and displayed reptiloid skin" (Blom et al., 2014). Neuroimaging revealed minor white-matter irregularities near the lentiform nucleus and semioval center but no other structural or functional abnormalities.

Although the case by Blom et al (2014) remains the sole published instance of non-acquired PMO, our laboratory is in contact with ten individuals who appear to have lifelong distortions. All report experiencing distortions for as long as they can remember, and several have a family history of facial distortions (see section 4.1). We refer to these cases as early-emerging PMO (EE-PMO). Their existence suggests that EE-PMO may be more prevalent than the literature indicates, much like developmental prosopagnosia was before a series of studies were published in the early twenty-first century (Mello & Duchaine, 2025). As is true of the case described below, it is often challenging to determine whether deficits in early-emerging disorders arise from early brain damage due to a neurological event or as a result of developmental processes that did not operate typically.

Here, we present the first comprehensive report of EE-PMO. Zed (stage name) has experienced persistent facial distortions and face recognition difficulties for as long as he can remember. His distortions are dynamic and vary in appearance and severity (see section 2.1 and Figure 1). To investigate Zed's condition, we conducted extensive behavioral assessments of his general visual perception, face perception and recognition, and object and voice perception and recognition. We also examined how different stimulus types and viewing conditions influenced the intensity of his facial distortions. Finally, we employed functional magnetic resonance imaging (fMRI) and diffusion tensor imaging (DTI) to explore the neural basis of Zed's atypical face processing.

2. Case report: zed

Zed, a 15-year-old boy at the time of behavioral testing, is right-handed and has a history of dyslexia, aphantasia, and color blindness. His mother describes him as independent and easygoing. In all interactions with our lab, Zed has been pleasant, and he occasionally displayed his quick wit and sense of humor. He attends high school, plays viola in a youth chamber orchestra, and enjoys history, cartography, and music.

Upon entering middle school (age 11), Zed was referred to a neuropsychologist for his dyslexia. The neuropsychological evaluation indicated that Zed's intellectual ability, theory of mind, memory, and visual-spatial ability were intact. However, he scored well below average on tests of face discrimination and recognition (5th percentile; Warrington Recognition Memory for Faces Test; Warrington, 1984) as well as long-term face memory (9th percentile; Delayed Warrington Recognition Memory for Faces Test), providing the first formal evidence of his difficulty with faces. Zed's struggles extend beyond face recognition, though, as he also experiences facial distortions. His mother

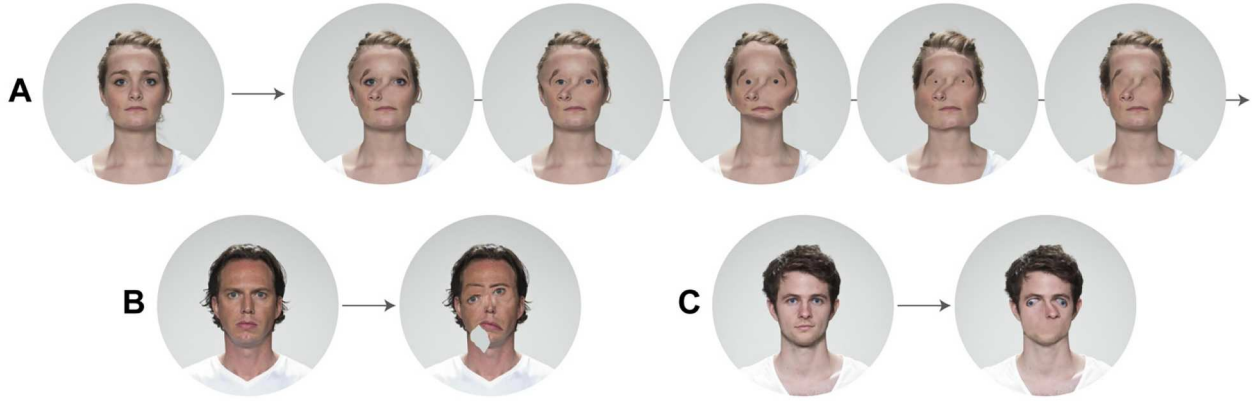


Figure 1. Visualizations of Zed's face distortions. (A) Stills from the dynamic visualization of one of Zed's distortions. To the left is the original face (DeBruine & Jones, 2017). Zed perceives the images on the timeline to the right morphing into one another over ~10 s. When describing these distortions, he said, "the chin grows and shrinks, and then the sides of the face follow … The nose is moved to the left … The eyebrows are rotated to the sides of the eyes. Oh, and the eyes disappeared slowly, with the corners first and then the iris and then the pupil." (B) A snapshot visualization of Zed's dynamic distortions. On the left is the original face, on the right is a visualization of Zed's distortions. Zed described this distortion in two steps. First, the "mouth droops down like it's hinging from the left corner … and I don't see anything in this [points to the grey area] section of the face. It's the same color as the background." Afterward, "the eyes are diagonal, with the left lower than the right … The eyebrows didn't follow but I think they're a little to the left." (C) A second snapshot visualization of Zed's dynamic distortions. On the left is the original face, on the right is a visualization of Zed's distortions. Zed described that "the eyes are drooping on both sides to the middle of the cheeks … The nose is curved to the right … and the mouth is completely gone."

recalls that as early as kindergarten, Zed mentioned seeing "curvy noses," "drooping eyes," and "disappearing features." These descriptions made it clear to her that Zed was seeing the world differently from others.

Zed is a fraternal twin and was born prematurely at 31 weeks gestational age by cesarean section, weighing 3 lbs. 5 oz. He stayed in the hospital for a month post-delivery and was treated for jaundice and provided with incubator care. After he was taken home from the hospital, Zed made good developmental progress, and he attained all developmental milestones within normal limits. Zed's family knows of no post-natal neurological events or brain trauma that could account for his distortions. However, none of Zed's family members have experienced similar visual distortions, so we suspect that his PMO may be a consequence of his premature birth.

In April 2023, Zed responded to our lab's online PMO questionnaire at https://prosopometamorphopsia.faceblind.org/. He wrote that "sometimes faces just don't look right I cannot describe it … it is a daily occurrence for as long as I can remember." After receiving his response, our lab met with Zed and his mother for an online interview in which he described his experiences. He noted that his distortions are usually bilateral and tend to include facial features moving, drooping, growing, shrinking, and disappearing. Faces in his periphery often appear as blank skin and are void of any facial features. Throughout Zed's testing, he has reported distortions on all full faces presented to him. Zed has also reported distortions in doll faces, symbolic faces, cars, animals, human bodies, and objects. Zed consistently reports dynamic distortions that change from moment to moment and typically emerge within three seconds of viewing a face. His distortions vary such that repeated presentations of the same face photograph yield different perceptual distortions. See section 2.1 and Supplementary Video S1 for information about the visualizations of Zed's dynamic distortions.

Unlike most PMO cases, Zed also experiences facial identity misrecognition, in which he sees incorrect identities when looking at others (Herald et al., 2023). These misrecognitions can manifest in various ways, such as seeing familiar faces on strangers or unfamiliar faces on familiar individuals. In some cases, these misrecognitions are extreme. For instance, while in public, Zed approached a person whom he thought was his mother—to him, the face appeared identical to hers. Although the person's clothes and hair were slightly different, Zed thought nothing of it. When he asked his sister, she pointed out that the individual was, instead, a male in his 60s. Even after the correction, Zed could not see the man's true appearance—he only saw his mother's face. These identity misrecognitions can occur multiple times per day. He often relies on hair to recognize and remember individuals, but when contextual cues are insufficient, he verifies with nearby friends or family before approaching someone he might know. At times, he has misrecognized himself in the mirror, stating it "doesn't look like me." Despite his distortions and misrecognitions, Zed is socially successful. He has friends at his high school, and he reports that he recognizes them via their hair, clothing, or body characteristics.

2.1. Distortion visualizations

Given the inherently subjective nature of PMO, accurately appreciating an individual's experience is challenging. Zed's distortions are dynamic and variable, which makes them especially difficult to describe to others. To give others a sense of what Zed experiences, we created the visualizations shown in Figure 1. As with most PMO cases, Zed sees distortions regardless of the viewing medium (e.g., photographs, television, or in-person; Mello et al., 2024). Therefore, Zed cannot be certain that the visualizations accurately represent his distortions. However, he believes that these visualizations are good approximations of the distortions he perceived and may help others better understand his experience.

The preliminary visualization procedure took place in person. We selected stimuli that consistently elicited severe distortions (refer to section 3.6.1). While looking at one image, he described each distortion he perceived, and we then manipulated a second image of the face to match his description. Throughout the in-person session, Zed provided feedback on the placement, size, and picture-plane orientation of each facial feature to achieve relatively accurate representations of each distortion. For the female face (seen in Fig 1A), which involved dynamic distortions, we followed the same procedure, with Zed providing detailed descriptions of the transitions between each distortion over time.

After the preliminary visualization procedure, each face was modified using Adobe Photoshop and After Effects. In a subsequent session, Zed reviewed the drafted visualizations and provided additional feedback. Despite perceiving additional distortions that impacted his perception of the visualizations, Zed still confidently offered constructive feedback regarding their accuracy. This feedback process continued until Zed felt that the visualizations effectively portrayed his experience. Refer to Video S1 for the photorealistic simulation of Zed's temporal distortions.

3. Methods and results

Following the initial screening, Zed remotely completed a background battery of standardized tests and questionnaires available online via Testable (Rezlescu et al., 2020). The control data, Zed's performance, and the statistical analyses conducted for these tests, as well as for others mentioned above, are presented in Supplementary Table S1. Written informed consent was obtained from all participants (Zed and controls), and this study was conducted in accordance with the Declaration of Helsinki.

3.1. Low-level vision testing

First, Zed's low-level visual abilities were assessed with the Hanover Early Vision Assessment (HEVA) (Kieseler et al., 2022), a computer-based battery comprising five three-alternative odd-one-out discrimination tasks that measure sensitivity to circle size, ellipse size, angle size, line length, and dot spacing. Each task consisted of 24 trials per task. For each trial, the three choices were presented for 1.5 s, and participants were asked to indicate which stimulus differed from the other two. Zed demonstrated intact low-level visual perception, scoring 75% correct on circle size (control mean = 75.27%, *SD* = 13.22%), 92% correct on ellipse size (control mean = 79.51%, *SD* = 12.95%), 83% correct on angular size (control mean = 74.35%, *SD* = 15.72%), 83% correct on line length (control mean = 83.71%, *SD* = 11.76%), and 83% correct on dot distance (control mean = 81.30%, *SD* = 12.52%), with a score of 83% overall (control mean = 78.83%, *SD* = 10.92%, *t* = 0.41).

During an in-person assessment, Zed correctly identified 5 out of 25 plates in the Ishihara Test (Ishihara, 1960), which detects red-green color deficiencies. His results were not specific to one particular type of color deficiency.

Zed's impaired color perception is also evidenced by his significantly elevated total error score of 164 (control mean = 65, *SD* = 14.70, *t* = −6.62) on the Farnsworth Munsell 100-Hue Test for Color Vision (Farnsworth, 1943; Kinnear, 2002), demonstrating impaired color discrimination ability.

To assess his visual imagery, Zed took the Visual Vividness Imagery Questionnaire (VVIQ) (Marks, 1973; Marks, 1995). The VVIQ asks individuals to imagine an object, scene, or friend, and rate the vividness of the image on a 5-point Likert scale. Zed scored significantly below controls with a mean rating of 1.25 out of 5 (control mean = 3.35, *SD* = 0.93, *t* = −2.25), indicating that he is aphantasic and lacks low-level sensory visual imagery (Friedlander et al., 2022; Keogh & Pearson, 2018).

3.2. Face detection

Next, we evaluated Zed's face detection, often considered the first stage of face processing (Crouzet et al., 2010; Tsao & Livingstone, 2008). He completed two two-tone forced-choice tasks designed to measure face detection ability. Additional statistical analyses for each measure are provided in Supplementary Table S1.

Face Mooney Forced-Choice: Zed's face detection ability was tested using the Face Mooney 3AFC, a forced-choice task in which he was presented with three two-tone images simultaneously for 3000 ms and asked to identify which image contained a face (Duchaine et al., 2023; Rezlescu et al., 2024). Zed scored normally for upright (82%, control mean = 87.5%, *SD* = 5.65%, *t* = −0.95) and inverted (64%, control mean = 61.2%, *SD* = 10.91%, *t* = 0.26) faces.

Two-tone Forced-Choice: Participants viewed three black-and-white stimuli simultaneously for 500 ms and were asked to select the stimulus that contained a face (Duchaine et al., 2023; Rezlescu et al., 2024). Zed scored significantly below controls on this assessment (82%, control mean = 95.8%, *SD* = 5.54%, *t* = −2.44), which suggests he may have difficulties with face detection.

3.3. Face recognition

To assess Zed's ability to recognize faces, he completed four face recognition tests. Figure 2 and Supplementary Table S1 provide additional information regarding statistical analyses, the control participants, and the control results for each of the face recognition measures.

Cambridge Face Memory Test (CFMT): The CFMT presents a series of six unfamiliar target faces before presenting test items that consist of three faces, one of which is one of the target faces (CFMT) (Duchaine & Nakayama, 2006). Zed's task was to pick out the target face. He scored significantly below the controls (56%, control mean = 80.4%, *SD* = 11%, *t* = −2.20).

Faces Old/New Test: Zed attempted to memorize 10 unfamiliar target faces, with each shown twice during the learning phase (Duchaine & Nakayama, 2005). Then, he was presented with 50 faces, one at a time: 20 old faces (10 target faces each presented twice) and 30 new faces. For each face, Zed indicated if it was old or new. These old/new results were quantified using A-prime, with values ranging from chance discrimination (0.5) to perfect discrimination (1.0). Zed's A-prime was 0.81, which is significantly below control scores (control mean A′ = 0.965, *SD* = 0.02, *t* = −7.53).

Famous Faces Test: Zed viewed 60 celebrity faces, which were closely cropped so only the face was

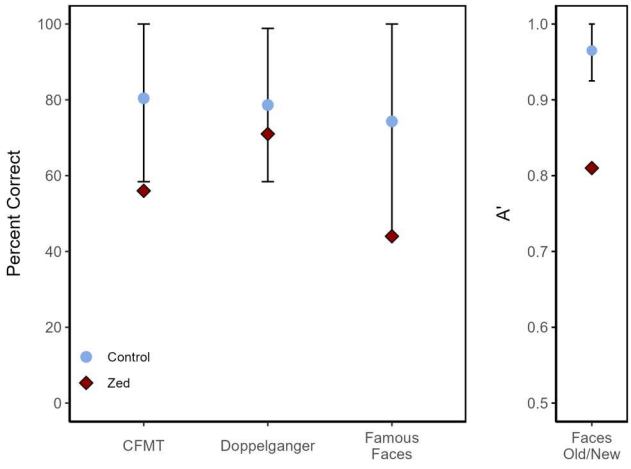


Figure 2. Results of the face recognition tests. Zed (red) scored significantly below controls (blue) on the CFMT and Faces Old/New Test, scored marginally below controls on the Famous Faces test, and scored within the normal range on the Doppelganger Test. Error bars represent ±2 standard deviations around the control mean.

visible (Kieseler & Duchaine, 2023). Of the 27 celebrities Zed was familiar with, he identified 44% of them correctly, which is about two standard deviations below the control mean, reaching marginal significance (control mean = 74.3%, *SD* = 15.1%, *t* = −1.94).

Doppelganger Test: In the Doppelganger Test, Zed was presented with the name of a famous person, followed by two simultaneously presented photos—one of the celebrity, and another of a lookalike of that celebrity (Kieseler & Duchaine, 2023). Zed correctly identified 71% of the 42 celebrities he was familiar with. This score was in the normal range (control mean = 78.6%, *SD* = 10.3%, *t* = −0.71).

3.4. Face perception

Zed's impaired face recognition performance motivated assessment of his face perception. This testing explored whether the recognition impairments arise due to face perception or face memory deficits. Additionally, these measures will allow assessment of the extent to which Zed's distortions impact judgments based on face perception. Please refer to Fig 3 and Supplementary Table S1 for additional information about each of the face perception measures.

Cambridge Face Perception Test (CFPT): Three aspects of Zed's face perception were evaluated using tests based on the format of the Cambridge Face Perception Test (CFPT) (Duchaine et al., 2007). Each assessment required Zed to sort faces by identity, age, or sex. In the CFPT-Identity, Zed attempted to arrange six facial images based on their similarity to a target face. The six images were created by morphing the target face with six unique faces in different proportions. Scores for each item were calculated by summing the deviations from the correct position for each face. For the CFPT-Age and CFPT-Sex, Zed was asked to sort morphed faces according to age or sex (refer to Supplementary Figures S1 and S2 for example stimuli). Zed

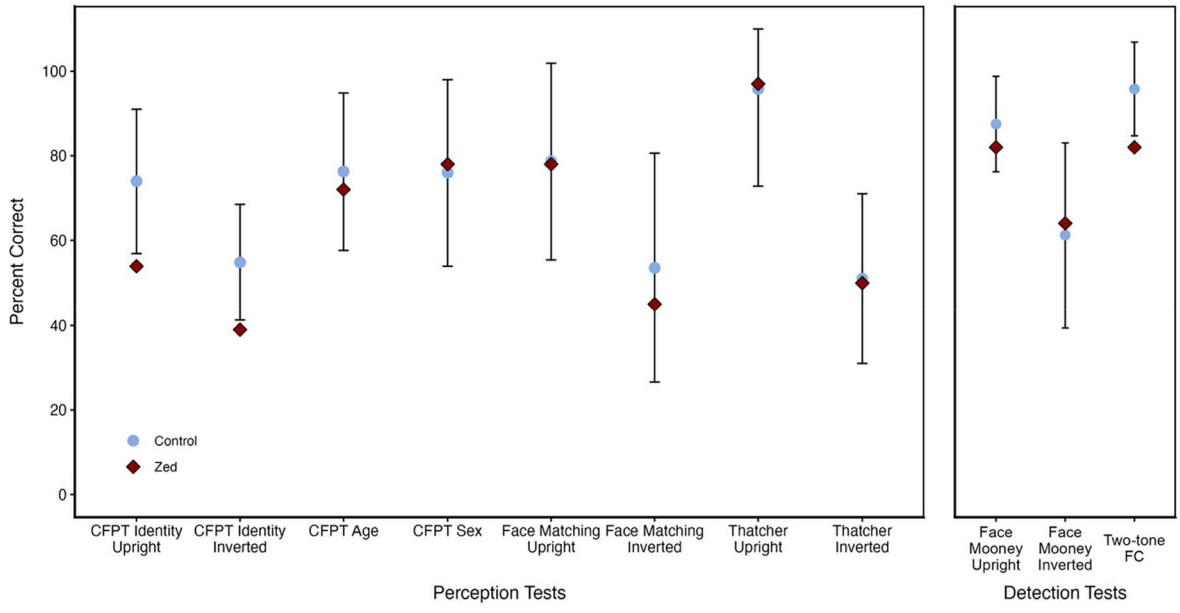


Figure 3. Results of face perception and detection tests. Zed scored (red) significantly below control means (blue) on CFTP Identity Upright and Inverted, and scored within a normal range across all other perception and detection tests. Error bars represent ±2 standard deviations around the control mean.

performed significantly below controls on the CFPT-Identity for upright (54%, control mean = 74.51%, *SD* = 8.47%, *t* = −2.35) and inverted (39%, control mean = 54.86%, *SD* = 6.80%, *t* = −2.30) faces. However, Zed performed normally on the CFPT-Age (72%, control mean = 76.3%, *SD* = 9.28%, *t* = −0.41) and CFPT-Sex (78%, control mean = 76%, *SD* = 11%, *t* = 0.15). These results indicate that Zed experiences difficulty with identity perception, but surprisingly, he appears to have normal sensitivity to characteristics that indicate age or sex differences.

Face Matching: In this matching task, a frontal view of a target face was presented for 600 ms, and then three faces were displayed from a different viewpoint for 4000 ms. Participants attempted to select the target face. Zed scored normally on the upright (78%, control mean = 78.7%, *SD* = 11.6%, *t* = −0.10) and inverted (45%, control mean = 53.6%, *SD* = 13.5%, *t* = −0.63) tasks.

Thatcher Test: In this task, two normal faces and one Thatcherized face were presented, and participants were asked to select the Thatcherized face. The Thatcherized faces had eyes, mouths, or both features rotated 180 degrees within the image (Duchaine et al., 2023). In upright faces, the inverted features are easy to detect, but when faces are inverted, the flipped features are difficult to notice (Thompson, 1980) (see Supplementary Figure S3 for example stimuli). Zed's scores were comparable to the controls' scores for upright (97%, control mean = 95.8%, *SD* = 11.5%, *t* = 0.07) and inverted (50%, control mean = 51%, *SD* = 10%, *t* = −0.10) faces.

3.5. Car recognition, perception, and detection and voice recognition

Zed completed car recognition, perception, and detection tasks to assess whether he has difficulties with object recognition, as well as a voice recognition task to evaluate his non-visual social recognition. For further information about the voice and car measures, see Supplementary Table S1.

Cars Old/New Test: This test used the same procedure as the Faces Old/New Test described above in Section 3.3 (Duchaine & Nakayama, 2005). Zed's A-prime was 0.85 (control mean = 0.94, *SD* = 0.04, *t* = −2.24), which is significantly below controls.

Cambridge Car Memory Test: The Cambridge Car Memory Test (Dennett et al., 2012) requires participants to learn six target cars and then select them from three-car forced-choice items. Zed performed in the low-normal range (56%, control mean = 70.6%, *SD* = 9.93%, *t* = −1.51).

Car Matching: Car perception was tested using the same procedure as the Face Matching est above in Section 3.4 (Rezlescu et al., 2024). Zed's score for upright car matching was normal (78%, control mean = 76.5%, *SD* = 10.1%, *t* = 0.10).

Car Mooney Forced-Choice: To test Zed's car detection, he was presented with three two-tone images simultaneously and asked to identify which image contained a car (Rezlescu et al., 2024). Zed's upright score was above the control average (90%, control mean = 75.1%, *SD* = 11.7%, *t* = 1.24).

Voices Old/New Test: Zed was tested with an old/new test for voices, in which he learned the voices of six female speakers (Garrido et al., 2009). After learning the voices, he was tested on his recognition of the voices and his ability to differentiate between them. Zed scored within the normal range on all tests of voice learning and recognition, with details in Supplementary Table S1.

3.6. Distortion testing

3.6.1. Multiview face distortion assessment

Previous studies of PMO have found that distortions may be modulated by how the faces are presented (Dalrymple et al., 2014). We created the Multiview Face Distortion Assessment (MFDA) using the Face Research Lab London Set (DeBruine & Jones, 2017), a publicly available face database, to assess the impact of five presentation variables on PMO distortions. Each participant is shown five sets of face images, each varying in one of the following dimensions: face viewpoint, picture-plane orientation, visual angle, visual field position, and facial features visible. Each set includes between 48 and 120 photographs. After viewing each face, participants rate the severity of their distortions on a Likert-type scale from 0 to 6 (0 = No distortion, 6 = Extreme distortion). Zed reported that his severity ratings typically reflected the number of distortions occurring simultaneously on a face.

As a control measure, every condition of the MFDA includes a frontal-view face presented at the center of the screen, where a participant's gaze is fixed. Across all frontal fixation faces, Zed's average distortion severity score was 2.85 out of 6, establishing Zed's baseline level of distortion severity when perceiving a face without varied viewpoints. Zed's distortions were not altered by changes in picture-plane orientation, visual angle, or viewpoint conditions (Supplementary Table S2). Thus, the results of these conditions are not discussed further.

In the visual field position condition, Zed fixated on a central cross and was presented with peripheral faces in the four quadrants of the screen. He experienced a 1.23-point increase in average distortion intensity rating

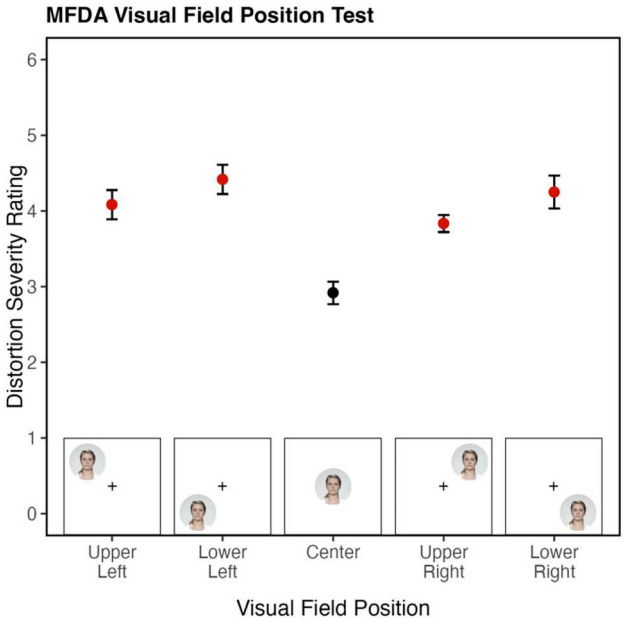


Figure 4. Results of the MFDA Visual Field Position Condition. Zed's distortion severity varies depending on the position of a face in his visual field. Peripheral faces (red) elicited more severe distortions than central faces (black). Error bars represent ±1 SEM. Ratings were made on a 0–6 Likert scale. Faces in the MFDA Visual Field Position Condition are from the Face Research Lab London Set (DeBruine & Jones, 2017), a publicly available face database.

when presented with frontal faces in his periphery (Center: $M = 2.92$, $SE = 0.14$; Periphery: $M = 4.15$, $SE = 0.094$). The intensity ratings at all four of the peripheral positions exceeded his average distortion severity rating for faces at fixation (Figure 4; Supplementary Table S3). These results indicate that faces in Zed's periphery are more distorted than those at fixation, consistent with Zed's reports of this phenomenon in daily life described in his Case Report (see Section 2).

In the visible facial features condition, Zed viewed different combinations of facial features at fixation. His distortion ratings for individual features were reduced (nose, left eye, right eye, mouth; Fig 5; Supplementary Tables S3 & S4), including 20% of trials with no distortions reported. Once two or more features were presented, Zed's average distortion intensity was comparable to that of the full face.

3.6.2. Familiar face test

The familiar face test sought to determine the impact of personal familiarity on Zed's distortion intensity, as some individuals with PMO experience distortions influenced by face familiarity (Heutink et al., 2012). This test was also motivated by Zed's frequent misidentifications of individuals in everyday life.

The familiar face test had 26 faces in total, 14 personally familiar and 12 unfamiliar. Each image was cropped

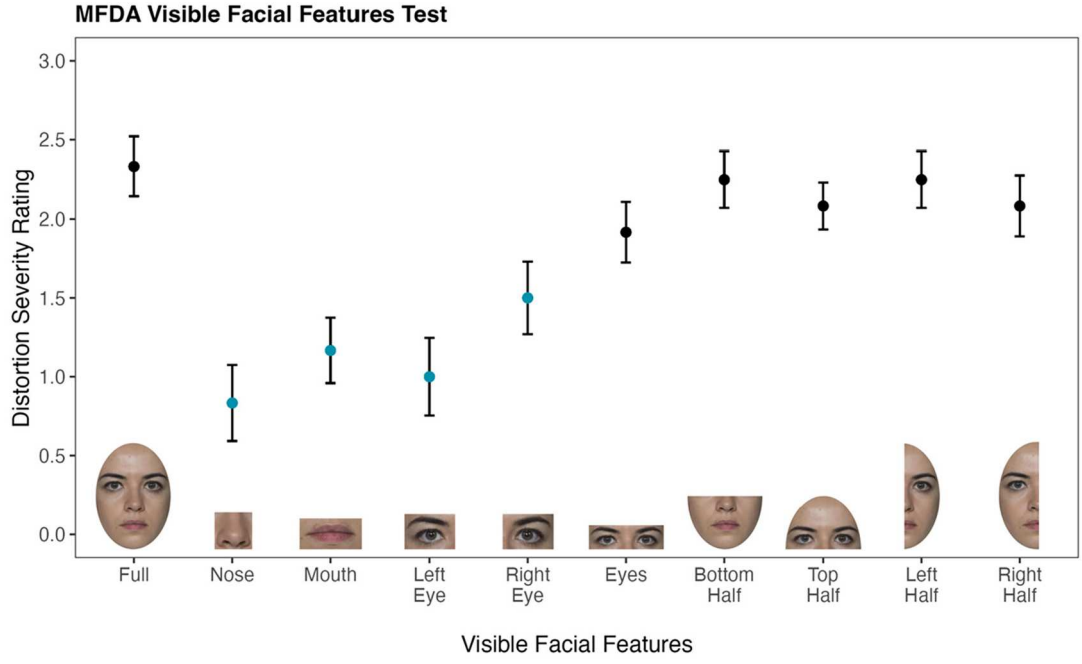


Figure 5. Results of the MFDA Visible Facial Features Condition. Zed's distortion severity ratings are influenced by combinations of visible features. The y-axis (0–3) reflects the range of Zed's ratings in this condition. Error bars represent ±1 SEM. Individual features (blue; nose, left eye, right eye, mouth) elicited less severe distortions than combined features or whole faces (black). Ratings were made on a 0–6 Likert scale. Faces in the MFDA Visible Facial Features Condition are cropped features from the Face Research Lab London Set (DeBruine & Jones, 2017), a publicly available face database.

around the face to exclude all hair and clothing. Each face was displayed four times, so 56 familiar and 48 unfamiliar stimuli were presented. The unfamiliar images, taken from face databases (Ebner et al., 2010; Egger et al., 2011; Ma et al., 2015), were slightly filtered to match the unprofessional photographic appearance of the familiar images. After viewing a face for 10 seconds, Zed rated his distortion severity on the 0–6 Likert scale described above and reported if the individual was familiar or unfamiliar. If the individual was familiar to Zed, he was prompted to name them.

Zed's ability to discriminate between familiar and unfamiliar faces was assessed using A-Prime (chance discrimination = 0.5; perfect discrimination = 1.0). Given that a typical individual can accurately recognize personally familiar faces with ease, Zed's A-prime score of 0.72 indicates difficulty discriminating between personally familiar and unfamiliar faces.

Zed stated that 88 of the 104 stimuli were familiar to him. His responses produced a hit rate of 92.7% (familiar face seen as familiar) and a false alarm rate of 75% (unfamiliar face seen as familiar). Of Zed's false alarms, only 55% were supported by a specific name, while the remainder included only contextual information (i.e., "someone from school"). In 36% of false alarms, the unfamiliar face was misidentified as a person he knows personally. While false alarms were Zed's primary deficit, Zed also had difficulty identifying the personally familiar individuals. Across 56 presentations of 14 personally familiar individuals, Zed identified 9 out of 14 with 100% accuracy, but the remaining 5 out of 14 with only 40% accuracy. There were no notable differences in closeness or familiarity between the people he recognized accurately and those he struggled with.

Zed's distortion severity rating did not differ by familiarity. Unfamiliar faces averaged 4.08 ($SD = 0.87$), while familiar faces averaged 3.91 ($SD = 0.67$). Additionally, his recognition ability did not differ by distortion severity rating (Correctly Recognized: $M = 4.14$, $SD = 0.62$; Incorrectly Recognized: $M = 3.83$, $SD = 0.77$). Thus, Zed shows no evidence of familiarity effects on distortion severity.

3.6.3. Objects

To assess the breadth of Zed's visual distortions, we tested him using an early version of the paradigm described by Kerns et al. (2025) with stimuli drawn from the THINGS database (Hebart et al., 2019). In this experiment, he was presented with images of 1280 everyday objects, body parts, animal faces, doll-faces, and inanimate-face images. Of the 1280 images originally presented, we analyzed only the 655 images that pictured a single unique category (face, object, body part, etc.). Images containing multiple categories were excluded because they often featured an object alongside a face or body part (e.g., shirt with part of face; watch with hand and wrist), potentially confounding distortion ratings.

In the main task, each image was presented individually for 10 seconds. After each image, Zed indicated whether he perceived a distortion by pressing one of two keys. The images were divided into three sessions.

Zed reported distortions in 31.31% of objects ($n = 559$) presented to him, comprising clothing accessories and decorations (41.38%, $n = 29$), tools, instruments, and equipment (37.83%, $n = 37$), plants and natural objects (41.67%, $n = 24$), food (30.80%, $n = 351$), and miscellaneous items (26.27%, $n = 118$). When Zed was presented with faces and body parts, distortion rates were higher: faces, dolls, and symbolic faces (100%, $n = 55$), animal faces (78.57%, $n = 14$), and body parts (92.59%, $n = 27$).

3.7. Neuroimaging

3.7.1. MRI / fMRI methods

Participants. Zed (age 16 at time of scanning) and 20 neurotypical participants (14 females, mean age = 33.86, $SD = 10.92$) participated in this portion of the study. An evaluation of the age differences between Zed and the control cohort is provided in section 4.4. Written informed consent was obtained from all participants in accordance with the Declaration of Helsinki. All procedures were approved by the Dartmouth College Committee for the Protection of Human Subjects.

Visual Stimuli and Task. To measure face selectivity, a functional localizer presented six classes of stimuli: faces, bodies, objects, phase-scrambled objects, natural scenes, and words (Stehr et al., 2025). Because of Zed's deficits with faces, our analysis focuses on face selectivity (though see Supplementary Figure S6 for word selectivity in visual word form area). Functional localizer stimuli consisted of dynamic video clips featuring various visual elements in motion, filmed against a uniform black backdrop to maximize contrast and visibility. Video clips subtended 26×15 degrees of visual angle in width and height. Participants viewed four runs, which each lasted 8 minutes and 22 seconds. Within each run, stimuli were grouped into 14-second single-category blocks containing five videos per block. Blocks of each category were displayed four times in each run in quasi-random order, twice in color and twice in grayscale. The trial order was the same for all participants. Throughout the experiment, participants were allowed to freely move their eyes and instructed to identify back-to-back repeats with a button press (1-

back task). Each of the four runs contained unique stimuli.

MRI Data Acquisition. Zed and the control participants were scanned at the Dartmouth Brain Imaging Center at Dartmouth College on a 3 Tesla Siemens Prisma MRI scanner (Siemens Medical Solutions) equipped with a 32-channel receive-only phased array head coil. High-resolution whole-brain anatomical images were collected using a T1-weighted magnetization-prepared rapid acquisition gradient echo (MPRAGE) sequence (208 sagittal slices; 1 mm isovoxel resolution, field of view = 256 mm; TR = 2,300 ms; TE = 2.03 ms; TI = 900 ms; flip angle = 9 degrees; FOV = 256 × 256 mm; bandwidth = 240 Hz/px).

Functional scans were acquired using a T2*-weighted gradient recalled echoplanar imaging multiband pulse sequence (cmrrmbep2bold) from the University of Minnesota's Center for Magnetic Resonance Research (69 slices; nominal spatial resolution 2 mm x 2 mm x 2 mm; 106 × 106 matrix size; 2 mm slice thickness, no-gap; field of view = 212 mm; phase partial Fourier scheme of 6/8; TR = 2,000 ms; TE = 30 ms; flip angle = 79 degrees; bandwidth = 1814Hz/Px; echo-spacing = 0.66 ms; excite pulse duration = 8,200 microseconds; multi-band factor = 3; phase encoding direction = AP; fat saturation on; advanced shim mode on; no iPat). Slices were oriented approximately in plane with the calcarine sulcus to ensure coverage of most, and often all, of the temporal, parietal, and occipital lobes. At the beginning of each session, a pair of EPI images with phase encoding directions of opposite polarity in the anterior-to-posterior plane were collected for post-hoc correction of EPI spatial distortion.

Stimulus Display and Scanner Peripherals. Stimuli were presented using a Panasonic PT-DW750BU 7000-Lumen WXGA DLP Projector and an SR Research in-bore back projection screen positioned just inside the head end of the magnet. Participants viewed the screen via a mirror mounted atop the head coil. The viewing distance was 127 mm from the eye to the mirror + 1,010 mm from the mirror to the screen = 1,137 mm total. The maximum square extent of the image projected on the screen was 297 mm x 297 mm. This resulted in a maximum possible visual angle of 14.97 degrees.

A Lenovo ThinkPad T480s computer running Linux Ubuntu 20.04.6 (Focal Fossa) controlled stimulus presentation and recorded button presses using MATLAB (R2021B) code and Psychtoolbox extensions. Behavioral responses from scanning sessions were collected using a Current Designs two-button fiber-optic handheld response pad, connected to a Current Designs 932 interface.

Preprocessing of fMRI data. All DICOM images were converted to NIfTI format using dcm2niix version 1.0.2018.11.25. From each participant's T1-weighted volume, cortical surface meshes of the pial-gray matter boundaries and gray matter-white matter boundaries were reconstructed using FreeSurfer's recon-all programme (Fischl & Dale, 2000; Dale et al., 1999; Fischl et al., 1999).

Subsequent pre-processing was performed using AFNI version 23.3.12 Septimius Severus (Cox, 1996) and AFNI's afni_proc.py. Slice timing differences were corrected, and non-linear geometric distortion correction was applied using separately acquired volumes where the phase-encoding direction was reversed (blip-up/blip-down strategy). EPI-anatomical alignment was carried out using the lpc + ZZ cost function while checking for possible left-right flips (Reynolds et al., 2023). Motion correction was applied, and the parameter estimates were stored for later use as nuisance regressors. Timepoints were censored when either the Euclidean norm exceeded 0.3 mm or when the outlier fraction exceeded 5%. Data were then iteratively smoothed to achieve a uniform smoothness of 4 mm FWHM (twice the EPI voxel dimension). The volumetric data was then projected onto the corresponding hemispheres of the high-density SUMA standard meshes (created from the FreeSurfer output with AFNI function @SUMA_Make_Spec_FS). Finally, each time series was scaled to units of local BOLD percent signal change. All pre-processing results were carefully visually inspected using the QC HTML reports generated by afni_proc.py (Reynolds et al., 2023).

Face-Selectivity Analysis. To estimate the face-selectivity of 14 face-selective areas in Zed and each control, we employed the following cross-validated procedure (Jiahui et al., 2018; Norman-Haignere et al., 2013). The four runs of the dynamic functional localizer were split into selection and test runs in a leave-one-run-out" method chosen to avoid issues of circularity. In each cross-validated fold, three runs were used for voxel selection, and the remaining run was used to compare the response to faces and objects. To select face-selective voxels, we computed the statistical contrast between blocks of faces and blocks of objects and windowed the results with seven different region of interest (ROI) masks in each hemisphere. Face-selective ROI masks included three ventral temporal regions (the occipital face area (OFA), the posterior fusiform face area (pFUS), and the medial fusiform face area (mFUS)), two lateral regions (the anterior superior temporal sulcus face area (aSTS) and the posterior superior temporal sulcus face area (pSTS)), and two regions of the extended face processing network (the anterior

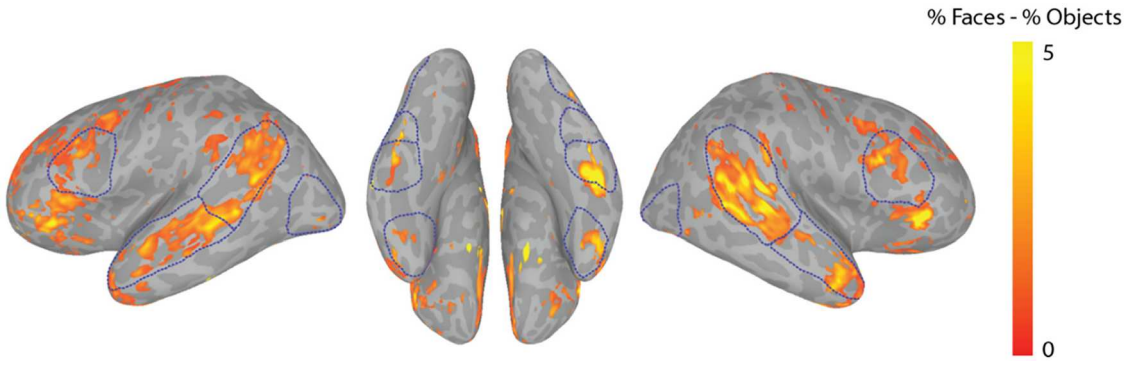


Figure 6. A whole-brain GLM analysis for Zed with colors indicating the difference in percent signal change for faces minus the percent signal change for objects following thresholding ($t > 3.3$, $p < 0.001$, uncorrected). Group-defined masks used for quantifying ROI-based face selectivity are outlined in blue. Group masks were drawn on the *fsaverage6* template and displayed on Zed's standardized meshes following alignment based on sulci and gyri.

temporal lobe face area (ATL) and the inferior frontal gyrus face area (IFG)). Masks were defined in group space (fsaverage6) based on face localizers collected from a group of 21 participants ($n = 13$ internal pilot participants viewing dynamic videos (Stehr et al., 2025; Pitcher et al., 2011; see Supplementary Video S2) and $n = 8$ Natural Scenes Dataset (Allen et al., 2022) participants viewing static images from the fLoc package (Stigliani et al., 2015)), all using a faces-versus-objects contrast. These broadly defined group masks served as anatomical anchors. Within these group masks, individual ROIs were tailored for Zed and each control participant by ranking voxels by their *t* value within the faces-versus-objects contrast across the three selection runs and extracting the top 10% highest-value voxels (Jiahui et al., 2018; Norman-Haignere et al., 2013). Within this set of selected voxels, we then measured the difference between beta coefficients (scaled to percent signal change) for face and object blocks in the left-out run. The final measure of category selectivity was the average of the measurements across all four cross-validated folds. Bayesian tests of deficits in the presence of covariates (Crawford et al., 2011) were used to test for differences between Zed's category selectivity and that of the 20 controls, controlling for variation related to age.

3.7.2. fMRI results

Figure 6 displays a whole-brain GLM contrasting blocks of faces versus blocks of objects for Zed. We found face-selective clusters of activity bilaterally in the inferior occipital gyrus, fusiform gyrus, superior temporal sulcus, anterior temporal lobe, and inferior frontal gyrus, with anatomical locations that are well aligned with previously studied nodes of the face-selective network (Duchaine & Yovel, 2015; Rosenke et al., 2021).

To quantitatively compare face selectivity in Zed and the neurotypical controls, we used the variable window method (Norman-Haignere et al., 2013) to examine the mean percent signal change to faces minus objects within the group-defined region of interest (ROI) masks (Jiahui et al., 2018) (Figure 7). Separate masks were created for the posterior and anterior aspects of the fusiform gyrus (pFUS/FFA-1 and mFUS/FFA-2, respectively) using the mid-fusiform sulcus as the separating border (Weiner et al., 2014). Bayesian tests for the presence of a deficit between Zed and the control group were conducted within each ROI, using age as a covariate of no interest (Crawford et al., 2011) (face selectivity as a function of age is plotted in Supplementary Figure S4). Compared to controls, Zed showed significant reductions in face selectivity in the right OFA ($Z_{ccc} = -2.01$, $p = 0.04$) and right pFUS ($Z_{ccc} = -2.82$, $p = 0.01$). The reduction in face selectivity was largest in right pFUS, with an estimated 99.02% of the population having greater face selectivity than Zed (CI: 93.89% to 99.995%). Inspection of the beta coefficients for individual categories (see Supplementary Fig S5) revealed Zed had similar activation for both faces and objects in right pFUS, so his decreased face selectivity resulted from a reduced response to faces rather than an elevated response to objects. Descriptive statistics, effect sizes, and interval estimates for all ROIs are presented in Table 1.

3.7.3. DTI methods

Data Acquisition and Preprocessing. Diffusion-weighted imaging (DWI) data were acquired from Zed and 78 healthy controls using a Siemens Magnetom Prisma 3 T scanner with a 32-channel head coil (Control dataset from [Jung et al., 2025]). Controls averaged 25.03 years of age ($SD = 5.25$) and ranged in age from 18 to 42. Forty-five were women, 31 were men, and two

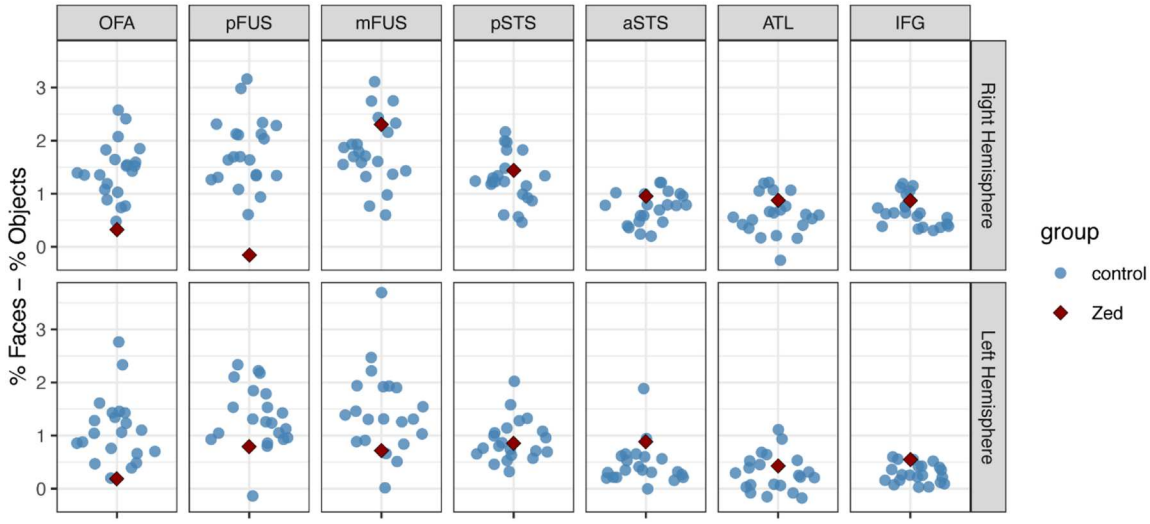


Figure 7. Face selectivity in Zed and Controls. Face selectivity expressed as percent signal change to faces minus percent signal change to objects for Zed and each control by ROI and hemisphere.

selected other gender (Jung et al., 2025). Technical difficulties with the anterior section of the head coil during Zed's scan resulted in reduced signal-to-noise ratio (SNR) in frontal brain regions. To minimize the risk of contamination from low-quality data, we excluded the anterior 4 cm of the brain from analysis (corresponding to ~22% of total brain length in MNI space, which spans 18 cm). As shown in the results, this exclusion did not appear to affect the comparison between Zed's results and those of the controls in the remaining ROIs.

The DWI protocol employed a multi-shell acquisition scheme with b-values of 0, 500, 1000, 2000, and 3000 s/mm^2, comprising 96 non-zero diffusion directions distributed as 6, 15, 15, and 60 directions across the respective shells. Data were acquired with 1.7 mm^3 isotropic voxels and preprocessed using MRtrix3, ANTs, and FSL. Standard preprocessing steps included quality control assessment, denoising, Gibbs ringing artifact removal, motion and distortion correction using top-up, and bias field correction. The preprocessed data were regridded to 1 mm^3 isotropic resolution for analysis.

Diffusion Model Fitting, ROI Analysis, and Statistical Comparisons. Diffusion tensor imaging (DTI) parameters were calculated using the b = 1000 s/mm^2 shell, generating maps of fractional anisotropy (FA), mean diffusivity (MD), axial diffusivity (AD), and radial diffusivity (RD1 and RD2). Following model fitting, all parametric maps were transformed to MNI standard space. Fifty-two white matter ROIs were defined using the Johns Hopkins University white matter atlas (Mori et al., 2008; Oishi et al., 2008), which was implemented

Table 1. ROI-based Bayesian tests of deficit comparing Zed to neurotypical controls. Abbreviated columns are defined as follows: Zed's mean delta % signal change (faces vs. objects), control mean delta % signal change (faces-vs-objects), control standard deviation (SD) of control delta % signal change (faces-vs-objects). Z_{ccc} = case—control effect size controlling for covariate of age. *P*-value is two-tailed.

ROI	Hemisphere	Zed Mean Δ% Signal Change	Control Mean Δ% Signal Change	Control *SD* Δ% Signal Change	Z_{ccc} (95% CI)	df	*p*-value	Estimated % of Population Below Zed (95% CI)
OFA	RH	0.33	1.45	0.52	−2.01 (−2.93, −0.92)	20	**0.04**	4.30 (0.17, 18.02)
OFA	LH	0.19	1.11	0.61	−1.49 (−2.39, −0.50)	20	0.10	9.83 (0.85, 30.74)
pFUS	RH	−0.14	1.78	0.63	−2.82 (−3.91, −1.55)	20	**0.01**	0.98 (0.01, 6.11)
pFUS	LH	0.80	1.33	0.58	−0.53 (−1.36, 0.31)	20	0.32	32.01 (8.66, 62.08)
mFUS	RH	2.30	1.80	0.63	1.05 (0.16, 1.89)	20	0.82	82.35 (56.26, 97.05)
mFUS	LH	0.72	1.46	0.77	−0.77 (−1.60, 0.09)	20	0.25	24.7 (5.48, 53.75)
pSTS	RH	1.44	1.27	0.47	0.66 (−0.21, 1.47)	20	0.72	72 (41.56, 92.93)
pSTS	LH	0.86	0.88	0.42	0.21 (−0.61, 1.03)	20	0.57	57.37 (27.16, 84.94)
aSTS	RH	0.96	0.73	0.29	1.97 (0.9, 2.91)	20	0.96	95.47 (81.59, 99.82)
aSTS	LH	0.88	0.44	0.40	1.92 (0.87, 2.87)	20	0.95	95.05 (80.84, 99.80)
ATL	RH	0.87	0.62	0.37	1.07 (0.16, 1.94)	20	0.83	82.78 (56.46, 97.38)
ATL	LH	0.43	0.30	0.34	0.80 (−0.07, 1.62)	20	0.76	76.01 (47.04, 94.72)
IFG	RH	0.88	0.65	0.29	0.46 (−0.39, 1.29)	20	0.66	65.81 (34.77, 90.05)
IFG	LH	0.55	0.29	0.18	1.33 (0.39, 2.20)	20	0.88	87.86 (65.13, 98.61)

in FSL. Mean values for each diffusion metric were then extracted for all participants.

Modified t-tests designed for single-case comparisons assessed whether Zed's values for each metric within each ROI differed significantly from the control group mean (Crawford et al., 2010; Crawford et al., 2011; Jung et al., 2025). To address multiple comparison issues arising from testing five metrics per ROI across 52 ROIs (260 comparisons), the false discovery rate (FDR) was controlled using the Benjamini-Hochberg procedure (Benjamini & Hochberg, 1995), with statistical significance defined as p-FDR < 0.05. Results were interpreted in the context of white matter microstructural integrity to identify regions where Zed's brain structure deviated from that of the controls.

3.7.4. DTI results

The DTI analysis involved five measures of white matter integrity (FA, MD, AD, RD1, RD2) for each of the 52 ROIs analyzed. In 49 ROIs, Zed's values across all five DTI measures did not differ significantly from those of the controls (see Supplementary Table S5). The predominance of normal values in the ROIs indicates that the head coil malfunction had minimal impact on the analyses. In contrast, significant differences in at least one measure were observed in three ROIs (Supplementary Table S5). The largest deviations were observed in the left inferior fronto-occipital fasciculus (IFOF; Figures 8 & 9; Supplementary Table S5), with differences in FA, MD, RD1, and RD2 consistent with reduced white matter integrity within this ROI. Additional significant differences were found for FA in the right anterior corona radiata and MD in a combined ROI consisting of the crus of the left fornix and left stria terminalis (see Supplementary Table S5).

4. Discussion

In this case study, we provide a comprehensive analysis of co-occurring EE-PMO and prosopagnosia by assessing

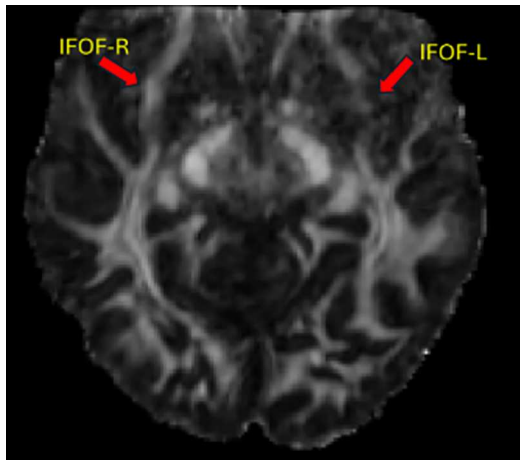


Figure 9. Reduced FA in Zed's Left IFOF. The FA value for Zed's left IFOF (IFOF-L) is significantly below that of the controls. Visual comparison of Zed's left IFOF and right IFOF (IFOF-R) makes this difference evident.

Zed's distortion severity, neuropsychological profile, face-selective areas, and white-matter characteristics. Zed experiences some of the most intense distortions documented in the literature, and he sees them on every face he encounters. Notably, despite his pronounced facial distortions, Zed scored normally when making perceptual judgments about face age and sex, highlighting a dissociation that warrants further investigation. Neuroimaging revealed Zed's facial distortions are accompanied by both abnormal white matter in the left IFOF and reduced face-selectivity in the right OFA and the right pFUS. Below, we discuss Zed's results, their implications, and some of the complications in interpreting findings from participants who experience facial distortions.

4.1. Early-emerging prosopometamorphopsia

Zed reports experiencing facial distortions, recognition difficulties, and misidentifications for as long as he can remember. Although his family is unaware of any neurological event that might have affected brain development, Zed's premature birth raises the possibility that his distortions reflect early neural injury rather than

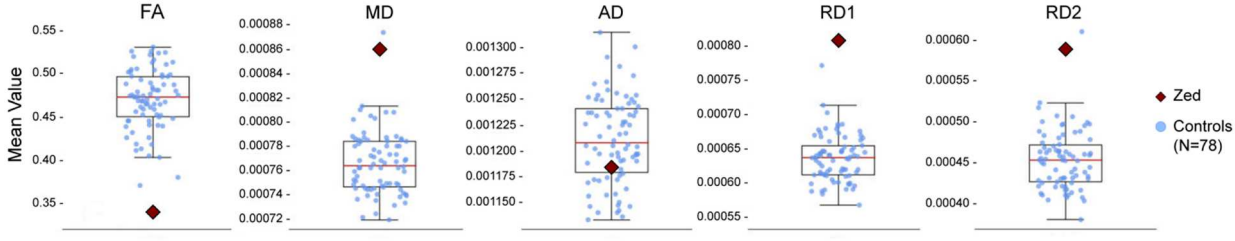


Figure 8. White matter abnormalities in Zed's left inferior fronto-occipital fasciculus. Four significant differences were found in the measurements of the left inferior fronto-occipital fasciculus.

atypical developmental processes. Multiple studies show that preterm individuals exhibit elevated rates of white matter abnormalities, and some of these studies suggest that the IFOF may be particularly vulnerable (Duerden et al., 2013; Kanel et al., 2021; Mouka et al., 2019; Mullen et al., 2011; Vollmer et al., 2017; Young et al., 2018). Given the uncertainty surrounding the origin of Zed's neural abnormalities, we refer to his case as early-emerging PMO rather than early-onset acquired PMO or developmental PMO.

Although Zed and the case reported by Blom et al. (2014) are the only published accounts to explicitly describe lifelong symptoms, our lab has heard from other EE-PMO cases, and we suspect that such cases are more common than the literature suggests. For instance, Ezri, a woman in her early thirties, experiences bilateral PMO that alters the shape and texture of faces (Mello et al., 2024). She cannot recall a time without these distortions. When Ezri shared her experiences with her mother, her mother recalled five or six instances in which she also saw salient facial distortions. Similarly, another woman has reported lifelong facial and body distortions. When she discussed her symptoms with her three teenage daughters, one described episodes in which her arms appeared unusually long, while another reported seeing distorted faces. These family histories suggest a potential genetic contribution to PMO. No such familial pattern, however, is present in Zed's case, as none of his family members report visual distortions.

In cases like Zed's in which early-emerging distortions are dynamic and varied, it seems likely that individuals will recognize that their perceptual experiences differ from those of others. However, if distortions in an early-emerging case are static and consistent across viewpoints and different faces, as has been observed in acquired PMO (Mello & Duchaine, 2025), individuals may not recognize their perceptions as distorted. Instead, we suspect that they are likely to interpret the altered features as accurate representations of others' faces, and they may never realize that their perception of faces is severely distorted.

4.2. Identity misrecognition

In addition to experiencing distortions, Zed frequently misrecognizes identities, identifying strangers as individuals he knows. After a misrecognition during an assessment, he noted, "I did not recognize the face even after you revealed the name. I still think it's the person I said it was." His misrecognitions can span differences in age, sex, and race, thus extending beyond what is typical of prosopagnosia. For instance, on the Familiar Face Test, he confidently identified a 70-year-old man as a 20-year-old woman. In another case described by his mother, he perceived a white man as black. While prosopagnosia may contribute to these errors, the marked differences between the actual face and the face he perceives, as well as the frequency with which he mistakenly sees familiar faces, suggest that these faces are being retrieved from memory during misrecognitions.

While no prior reports document frequent misrecognitions across age, sex, or race to the extent observed in Zed, several studies describe similar identity misrecognitions. Following a right middle cerebral artery infarction, one man reported repeated misidentifications of unfamiliar individuals as family or friends, despite performing relatively well on sex, age, and face matching tasks—similar to Zed (Sugahara et al., 2022). Unlike Zed, however, this individual also struggled to recognize familiar voices. In a more extreme case, a prosopagnosic woman with hallucinatory facial palinopsia found that, after briefly looking at a poodle on the bus, all of the passengers' faces had transformed into that of a poodle (Landis et al., 1986). Intracranial stimulation studies have also elicited phenomena resembling Zed's distortions and misrecognitions, with stimulation of the right fusiform face area (FFA) inducing both facial distortions and feelings of familiarity. In one case, a patient reported facial drooping and that the face "almost looks like somebody I've seen before" (Parvizi et al., 2012). Similarly, another patient described seeing the eyes, mouth, and mole of a previously presented face superimposed atop a new face following right FFA stimulation (Jonas et al., 2018). In a separate trial, the patient reported that the face had "eyes and ears which were not theirs" but could not match familiar identities to these features. Notably, Zed's right pFUS also exhibited marked functional anomalies, suggesting that these neural irregularities may underlie his misrecognition experiences.

4.3. PMO and face perception

Given that PMO is defined as a disorder of face perception, we evaluated Zed's performance on face perception and detection tasks. Surprisingly, despite his pronounced facial distortions, Zed performed within the normal range on four out of five face perception measures and showed difficulty only with the CFPT-Identity, which required sorting based on facial identity. Zed's normal performance on the CFPT-Age and CFPT-Sex was particularly unexpected. Good performance on these tests requires extended, close scrutiny of the subtle age- or sex-related differences between faces

and a level of perceptual precision that we anticipated would be disrupted by his distortions.

Zed's results suggest a potential dissociation between accurate explicit perceptual judgments and distorted conscious perceptual experience, but additional work is necessary to establish this dissociation and investigate the underlying processes. It may be that Zed's normal performance on the perceptual tests reflects the temporal course of his distortions, with distortions emerging within three seconds of viewing a face. He may make explicit perceptual judgments during this brief window, prior to the distortions becoming more severe. To explore this possibility in future studies, Zed could be asked to detect the endpoints of a face morph continuum that gradually changes from one face to another (e.g., from an androgynous face toward a more male or female endpoint). With this sort of stimulus, his distortions should be at full severity by the time information is available to support his judgments. If his judgments are unaffected by his distortions, Zed should identify the trajectory of face shifts as rapidly as control participants.

Theoretically, Zed's explicit judgments could also be driven by preserved local feature processing, while dysfunctional holistic processing might trigger the severe distortions he experiences. Crucially, the accurate feature-level perception would remain intact and accessible, allowing for accurate explicit judgments about faces, even when distortions are present. Consistent with this feature processing account, Zed's responses appear to indicate that he experiences reduced distortion severity when viewing individual features in the MFDA facial feature study. Zed's normal performance on the Thatcher test, which requires perception of localized structural rotations (such as flipped eyes or mouths), is also consistent with intact feature processing that might allow him to succeed in this task despite his distortions on both upright and inverted faces. However, while we find this hypothesis an intriguing possibility, far more evidence about the relationship between conscious face perception and face perception judgments is required before confident conclusions can be drawn.

To explore Zed's distortions with inverted faces, we tested whether his distortion severity was modulated by orientation within the MFDA picture-plane orientation condition (across 8 different degrees of rotation). Zed's distortion ratings for inverted faces, with an average severity of 2.92 ($SD = 0.90$), were comparable to his average rating for upright faces of 2.75 ($SD = 0.45$). The similarity of these scores tentatively suggests that Zed's upright face distortions are driven in large part by face processes that are applied to both upright and inverted faces (Moscovitch et al., 1997; Rivest et al., 2009). Comparable distortions for both upright and inverted faces have been reported for other PMO participants (Almeida et al., 2020; Mello et al., 2025), though this is not a universal feature in PMO (Dalrymple et al., 2014).

However, because inverted faces appear to depend on processes that contribute to object perception (Moscovitch et al., 1997; Pitcher et al., 2011) and Zed occasionally experiences object distortions, his inverted face distortions may have an alternative origin. When presented with objects from the THINGS database (Hebart et al., 2019) using a paradigm derivative of that used in Kerns et al. (2025), Zed reported seeing distortions in approximately one-third of objects presented to him. When viewing an inverted face, the visual system may treat it similarly to a complex non-face object (Moscovitch et al., 1997; Rivest et al., 2009); thus, the distortions Zed sees in inverted faces could involve the same disrupted object-processing streams that cause his object distortions.

4.4. Neural correlates of zed's face distortions and prosopagnosia

To investigate the neural correlates of Zed's distortions, we carried out functional and structural imaging. A functional localizer assessing face-selective areas revealed that Zed exhibited notable reductions in two regions: the right occipital face area (OFA) and the right posterior fusiform face area (pFUS). Whole-brain analyses revealed that Zed recruited canonical face-selective regions—including the bilateral inferior occipital gyrus (OFA), fusiform gyrus (FFA), superior temporal sulcus (STS), anterior temporal lobe, and inferior frontal gyrus. However, quantitative comparisons with neurotypical controls revealed significantly reduced face selectivity in key nodes of this network, specifically within the right OFA and, most notably, the right pFUS. Inspection of Zed's beta coefficients to faces and objects showed that this reduced face selectivity resulted from an attenuated response to faces rather than an unusually strong response to objects.

Because our neurotypical fMRI control group was older than Zed, it is important to consider whether Zed's reduced face selectivity could be attributed to this difference. Neuroimaging studies have shown that face-selective regions in the ventral visual stream, particularly the right FFA and OFA, undergo structural development through adolescence and into early adulthood (Golarai et al., 2010; Gomez et al., 2017). However, by mid-adolescence (age 11–16), these regions already exhibit robust, well-established face selectivity (Golarai et al., 2007; Scherf et al., 2007). Given that Zed was 16

during the time of scanning, his significant reductions in face selectivity are unlikely to be a function of his age. This is illustrated in Supplementary Figure S4, which tracks the relationship between age and face selectivity (faces minus objects percent signal change). When mapping Zed against the control group's regression slopes, his selectivity scores in the right pFUS and right OFA fall outside the standard error of the mean, which indicates that his neural profile is abnormal even when accounting for age-related variance.

The abnormalities observed in Zed's right posterior face regions are notable, given evidence that intracranial stimulation of these face-selective areas can alter conscious perception of faces. Direct intracranial stimulation of the right OFA and right pFUS has repeatedly altered and distorted face perception and recognition (Jonas et al., 2012; Jonas et al., 2014; Jonas et al., 2018; Mundel et al., 2003; Parvizi et al., 2012; Rangarajan et al., 2014; Schalk et al., 2017; Schrouff et al., 2020). In contrast, stimulation of face-selective regions in the left hemisphere only rarely alters conscious face perception (Rangarajan et al., 2014), and stimulation of anterior face regions in the right hemisphere disrupts the ability to recognize facial identity without affecting facial perception (Jonas et al., 2015; Jonas & Rossion, 2021). These intracranial findings suggest that right OFA and right pFUS play particularly critical roles in the distortions observed in PMO cases, consistent with Zed's results. While stimulation represents an internal disruption to the face network, similar perceptual abnormalities can be driven via external stimulus manipulations. Behaviorally, the flashed face distortion effect (Tangen et al., 2011) induces shape-based distortions by presenting faces in rapid succession in an individual's periphery. The strength of this effect has been shown to correlate proportionally with activity in the right FFA and right OFA (Wen & Kung, 2014), reinforcing that these right-hemisphere face-selective regions contribute to face distortions.

In addition to functional abnormalities, Zed also exhibited white-matter deficits in three ROIs. The ROI with the clearest reductions in white matter integrity was the left inferior fronto-occipital fasciculus (IFOF). Two other ROIs, the right anterior corona radiata and a combined ROI consisting of the crus of the left fornix and left stria terminalis, also suggested reductions in white matter integrity, but given their functional roles, they appear unlikely to contribute to Zed's distortions. On the other hand, deficits in the left IFOF could be linked to visual distortions. The IFOF is a ventral white matter tract projecting between the occipital and frontal lobes (Catani & Thiebaut de Schotten, 2008) and is a crucial contributor to the language network and semantic speech processing (Conner et al., 2018; Motomura et al., 2014). Subcortical stimulation of the dorsal IFOF has resulted in alexia (pure word blindness) and agraphia (loss of writing ability) (Motomura et al., 2014). In addition, some suggest it may be involved in face processing (Taddei et al., 2012; Philippi et al., 2009). In adolescents, Taddei et al. (2012) found significant correlations between IFOF FA values and normalized N400 amplitude in response to angry faces. Additionally, Philippi et al. (2009) found that damage to the right IFOF predicted facial emotion recognition impairments for negative emotions such as sadness, anger, and fear. Given the IFOF's multifaceted role in semantic language processing *and* face processing, this deficit may be involved in Zed's comorbid dyslexia, face recognition difficulties, and face distortions. While our current structural analysis focused on large-scale tracts, future work with a larger PMO cohort will evaluate localized white matter in category-selective areas (e.g., right OFA and pFUS) to further explore the neuroanatomical factors in PMO.

4.5. Zed's comorbid conditions

Results from Zed's behavioral and neuropsychological testing are consistent with both EE-PMO and prosopagnosia. Although PMO is more frequently reported in individuals with prosopagnosia (Herald et al., 2023), face recognition typically remains intact in PMO (Blom et al., 2014; Herald et al., 2023), even in cases of bilateral and pronounced facial distortions (Blom et al., 2014; Blom et al., 2021; Hwang et al., 2012). Thus, we believe Zed's difficulties with facial recognition on the CFMT, the Faces Old/New Test, the Familiar Face Test, the Famous Faces Test, and the CFPT-Identity are best attributed to his prosopagnosia rather than his EE-PMO. Zed's performance on the Doppelganger Test, however, fell within the average control range. At present, we do not have an explanation for this discrepancy among face recognition tasks. In the future, we hope to collect additional data with Zed to determine if this is a reliable finding.

Beyond EE-PMO, the co-occurrence of Zed's prosopagnosia, aphantasia, and dyslexia introduces additional complexity. These conditions frequently co-occur; for example, individuals with developmental prosopagnosia report reduced visual imagery (Grüter et al., 2009), and those with aphantasia exhibit impairments in face memory despite intact face matching (Pounder et al., 2026). Face-processing difficulties are also documented in individuals with dyslexia (Sigurdardottir et al., 2021). Ultimately, Zed's processing difficulties plausibly reflect compounding contributions from his dyslexia,

aphantasia, prosopagnosia, and EE-PMO, though further evidence is required to draw firmer conclusions as to which behavioral outcomes are attributable to each specific condition.

Acknowledgements

We thank Zed for his dedicated participation and his family for their support during this study. Gemini 3 (Google) and Claude Sonnet 5.5 (Anthropic) were used to polish the grammar of this manuscript and to check in-text citations against the reference list for errors. The authors reviewed and verified all AI-suggested changes against original references and take full responsibility for the content of this article.

Author contributions

CRediT: **Sydney Fortner:** Conceptualization, Data curation, Formal analysis, Funding acquisition, Investigation, Methodology, Project administration, Visualization, Writing – original draft, Writing – review & editing; **Antônio Mello:** Conceptualization, Formal analysis, Methodology, Writing – review & editing; **Daniel Stehr:** Data curation, Formal analysis, Investigation, Methodology, Visualization, Writing – review & editing; **Chandana Kodiweera:** Formal analysis, Visualization, Writing – review & editing; **Heejung Jung:** Formal analysis, Investigation; **Sarah Kerns:** Investigation; **Krzysztof Bujarski:** Investigation; **Tor Wager:** Funding acquisition, Supervision; **Brad Duchaine:** Conceptualization, Funding acquisition, Methodology, Supervision, Writing – review & editing.

Disclosure statement

No potential conflict of interest was reported by the authors.

Funding

This work was supported by the Hitchcock Foundation Grant (B.D.), the National Eye Institute (B.D.: R01EY030613), Dartmouth College UGAR Honors Thesis Grant (S.F.), and the National Institute of Mental Health (T.W.: 5R37MH076136).

Data availability statement

All neuropsychological, behavioral, and control data (collected on Prolific) are available on the Open Science Framework (OSF): https://osf.io/d5ej9/?view_only=328304d992514be4b200137101a5347c. Zed's DTI and fMRI data are available on OpenNeuro: https://openneuro.org/datasets/ds006592. Control DTI are available on OpenNeuro under sub-0XXX/ses-01/dwi https://openneuro.org/datasets/ds005256/versions/1.1.0. Control fMRI data are available on OpenNeuro: https://openneuro.org/datasets/ds006472.

ORCID

Sydney Fortner http://orcid.org/0009-0009-9345-8857
Antônio Mello https://orcid.org/0000-0002-2980-696X
Daniel Stehr https://orcid.org/0000-0003-1673-3260
Chandana Kodiweera https://orcid.org/0000-0002-6576-8534
Heejung Jung https://orcid.org/0000-0001-5839-1655
Sarah Kerns https://orcid.org/0009-0001-7441-1828
Krzysztof Bujarski https://orcid.org/0000-0002-1329-5085
Tor Wager https://orcid.org/0000-0002-1936-5574
Brad Duchaine https://orcid.org/0000-0002-2754-2964

References

Allen, E. J., St-Yves, G., Wu, Y., Breedlove, J. L., Prince, J. S., Dowdle, L. T., Nau, M., Caron, B., Pestilli, F., Charest, I., Hutchinson, J. B., Naselaris, T., & Kay, K. (2022). A massive 7 T fMRI dataset to bridge cognitive neuroscience and artificial intelligence. *Nature Neuroscience*, *25*(1), 116–126. https://doi.org/10.1038/s41593-021-00962-x

Almeida, J., Freixo, A., Tábuas-Pereira, M., Herald, S. B., Valério, D., Schu, G., Duro, D., Cunha, G., Bukhari, Q., Duchaine, B., & Santana, I. (2020). Face-Specific perceptual distortions reveal A view- and orientation-independent face template. *Current Biology*, *30*(20), 4071–4077. https://doi.org/10.1016/j.cub.2020.07.067

Benjamini, Y., & Hochberg, Y. (1995). Controlling the false discovery rate: A practical and powerful approach to multiple testing. *Journal of the Royal Statistical Society: Series B (Methodological)*, *57*(1), 289–300. https://doi.org/10.1111/j.2517-6161.1995.tb02031.x

Blom, J. D., Sommer, I. E. C., Koops, S., & Sacks, O. W. (2014). Prosopometamorphopsia and facial hallucinations. *The Lancet*, *384*(9958), 1998. https://doi.org/10.1016/S0140-6736(14)61690-1

Blom, J. D., Ter Meulen, B. C., Dool, J., & Ffytche, D. H. (2021). A century of prosopometamorphopsia studies. *Cortex*, *139*, 298–308. https://doi.org/10.1016/j.cortex.2021.03.001

Castaldi, E., Piazza, M., & Iuculano, T. (2020). Learning disabilities: Developmental dyscalculia. *Handbook of Clinical Neurology*, *174*, 61–75. https://doi.org/10.1016/B978-0-444-64148-9.00005-3

Catani, M., & Thiebaut de Schotten, M. (2008). A diffusion tensor imaging tractography atlas for virtual in vivo dissections. *Cortex*, *44*(8), 1105–1132. https://doi.org/10.1016/j.cortex.2008.05.004

Conner, A. K., Briggs, R. G., Sali, G., Rahimi, M., Baker, C. M., Burks, J. D., Glenn, C. A., Battiste, J. D., & Sughrue, M. E. (2018). A connectomic atlas of the human cerebrum—chapter 13: Tractographic description of the inferior fronto-occipital fasciculus. *Operative Neurosurgery*, *15*(suppl_1), S436–S443. https://doi.org/10.1093/ons/opy267

Cox, R. W. (1996). AFNI: Software for analysis and visualization of functional magnetic resonance neuroimages. *Computers and Biomedical Research*, *29*(3), 162–173. https://doi.org/10.1006/cbmr.1996.0014

Crawford, J. R., Garthwaite, P. H., & Porter, S. (2010). Point and interval estimates of effect sizes for the case-controls design in neuropsychology: Rationale, methods, implementations, and proposed reporting standards. *Cognitive Neuropsychology*, *27*(3), 245–260. https://doi.org/10.1080/02643294.2010.513967

Crawford, J. R., Garthwaite, P. H., & Ryan, K. (2011). Comparing a single case to a control sample: Testing for neuropsychological deficits and dissociations in the presence of covariates. *Cortex*, *47*(10), 1166–1178. https://doi.org/10.1016/j.cortex.2011.02.017

Critchley, M. (1953). *The parietal lobes (pp. Vii, 480)*. Williams and Wilkins.

Crouzet, S. M., Kirchner, H., & Thorpe, S. J. (2010). Fast saccades toward faces: Face detection in just 100 ms. *Journal of Vision*, *10*(4), 16. https://doi.org/10.1167/10.4.16

Dale, A. M., Fischl, B., & Sereno, M. I. (1999). Cortical Surface-Based Analysis. *NeuroImage*, *9*(2), 179–194. https://doi.org/10.1006/nimg.1998.0395

Dalrymple, K. A., Davies-Thompson, J., Oruc, I., Handy, T. C., Barton, J. J. S., & Duchaine, B. (2014). Spontaneous perceptual facial distortions correlate with ventral occipitotemporal activity. *Neuropsychologia*, *59*, 179–191. https://doi.org/10.1016/j.neuropsychologia.2014.05.005

DeBruine, L., & Jones, B. (2017). Face Research Lab London Set (Version 5) [Data set]. figshare. https://doi.org/10.6084/m9.figshare.5047666.v5

Dennett, H. W., McKone, E., Tavashmi, R., Hall, A., Pidcock, M., Edwards, M., & Duchaine, B. (2012). The Cambridge car memory test: A task matched in format to the Cambridge face memory test, with norms, reliability, sex differences, dissociations from face memory, and expertise effects. *Behavior Research Methods*, *44*(2), 587–605. https://doi.org/10.3758/s13428-011-0160-2

Duchaine, B., Germine, L., & Nakayama, K. (2007). Family resemblance: Ten family members with prosopagnosia and within-class object agnosia. *Cognitive Neuropsychology*, *24*(*4*), 419–430. https://doi.org/10.1080/02643290701380491

Duchaine, B., & Nakayama, K. (2005). Dissociations of face and object recognition in developmental prosopagnosia. *Journal of Cognitive Neuroscience*, *17*(2), 249–261. https://doi.org/10.1162/0898929053124857

Duchaine, B., & Nakayama, K. (2006). The Cambridge face memory test: Results for neurologically intact individuals and an investigation of its validity using inverted face stimuli and prosopagnosic participants. *Neuropsychologia*, *44*(4), 576–585. https://doi.org/10.1016/j.neuropsychologia.2005.07.001

Duchaine, B., Rezlescu, C., Garrido, L., Zhang, Y., Braga, M. V., & Susilo, T. (2023). The development of upright face perception depends on evolved orientation-specific mechanisms and experience. *iScience*, 107763. https://doi.org/10.1016/j.isci.2023.107763

Duchaine, B., & Yovel, G. (2015). A revised neural framework for face processing. *Annual Review of Vision Science*, *1*(1), 393–416. https://doi.org/10.1146/annurev-vision-082114-035518

Duerden, E. G., Card, D., Lax, I. D., Donner, E. J., & Taylor, M. J. (2013). Alterations in frontostriatal pathways in children born very preterm. *Developmental Medicine & Child Neurology*, *55*(10), 952–958. https://doi.org/10.1111/dmcn.12198

Ebner, N. C., Riediger, M., & Lindenberger, U. (2010). FACES - A database of facial expressions in young, middle-aged, and older women and men: Development and validation. *Behavior Research Methods*, *42*(1), 351–362. https://doi.org/10.3758/BRM.42.1.351

Egger, H. L., Pine, D. S., Nelson, E., Leibenluft, E., Ernst, M., Towbin, K. E., & Angold, A. (2011). The NIMH child emotional faces picture set (NIMH-ChEFS): A new set of children's facial emotion stimuli. *International Journal of Methods in Psychiatric Research*, *20*(3), 145–156. https://doi.org/10.1002/mpr.343

Farnsworth, D. (1943). The Farnsworth-Munsell 100-Hue and dichotomous tests for color vision*. *JOSA*, *33*(10), 568–578. https://doi.org/10.1364/JOSA.33.000568

Fischl, B., & Dale, A. M. (2000). Measuring the thickness of the human cerebral cortex from magnetic resonance images. *Proceedings of the National Academy of Sciences*, *97*(20), 11050–11055. https://doi.org/10.1073/pnas.200033797

Fischl, B., Sereno, M. I., & Dale, A. M. (1999). Cortical Surface-Based Analysis. *NeuroImage*, *9*(2), 195–207. https://doi.org/10.1006/nimg.1998.0396

Friedlander, K. J., Lenton, F. H., & Fine, P. A. (2022). A multifactorial model of visual imagery and its relationship to creativity and the vividness of visual imagery questionnaire. *Psychology of Aesthetics, Creativity, and the Arts*, 829–847. https://doi.org/10.1037/aca0000520

Garrido, L., Eisner, F., McGettigan, C., Stewart, L., Sauter, D., Hanley, J. R., Schweinberger, S. R., Warren, J. D., & Duchaine, B. (2009). Developmental phonagnosia: A selective deficit of vocal identity recognition. *Neuropsychologia*, *47*(*1*), 123–131. https://doi.org/10.1016/j.neuropsychologia.2008.08.003

Golarai, G., Ghahremani, D. G., Whitfield-Gabrieli, S., Reiss, A., Eberhardt, J. L., Gabrieli, J. D. E., & Grill-Spector, K. (2007). Differential development of high-level visual cortex correlates with category-specific recognition memory. *Nature Neuroscience*, *10*(4), 512–522. https://doi.org/10.1038/nn1865

Golarai, G., Liberman, A., Yoon, J. M. D., & Grill-Spector, K. (2010). Differential development of the ventral visual cortex extends through adolescence. *Frontiers in Human Neuroscience*, *3*, Article 80. https://doi.org/10.3389/neuro.09.080.2009

Gomez, J., Barnett, M. A., Natu, V., Mezer, A., Palomero-Gallagher, N., Weiner, K. S., Amunts, K., Zilles, K., & Grill-Spector, K. (2017). Microstructural proliferation in human cortex is coupled with the development of face processing. *Science*, *355*(6320), 68–71. https://doi.org/10.1126/science.aag0311

Grüter, T., Grüter, M., Bell, V., & Carbon, C.-C. (2009). Visual mental imagery in congenital prosopagnosia. *Neuroscience Letters*, *453*(3), 135–140. https://doi.org/10.1016/j.neulet.2009.02.021

Hebart, M. N., Dickter, A. H., Kidder, A., Kwok, W. Y., Corriveau, A., Wicklin, C. V., & Baker, C. I. (2019). THINGS: A database of 1,854 object concepts and more than 26,000 naturalistic object images. *PLoS One*, *14*(10), e0223792. https://doi.org/10.1371/journal.pone.0223792

Herald, S. B., Almeida, J., & Duchaine, B. (2023). Face distortions in prosopometamorphopsia provide new insights into the organization of face perception. *Neuropsychologia*, *182*, 108517. https://doi.org/10.1016/j.neuropsychologia.2023.108517

Heutink, J., Brouwer, W. H., Kums, E., Young, A., & Bouma, A. (2012). When family looks strange and strangers look normal: A case of impaired face perception and recognition after stroke. *Neurocase*, *18*(1), 39–49. https://doi.org/10.1080/13554794.2010.547510

Hwang, J. Y., Ha, S. W., Cho, E. K., Han, J. H., Lee, S. H., Lee, S. Y., & Kim, D. E. (2012). A case of prosopometamorphopsia

restricted to the nose and mouth with right medial temporooccipital lobe infarction that included the fusiform face area. *Journal of Clinical Neurology (Seoul, Korea)*, *8*(4), 311–313. https://doi.org/10.3988/jcn.2012.8.4.311

Ishihara, S. (1960). Tests for colour-blindness. *Kanehara Shuppan Company Japan, 5th*.

Jiahui, G., Yang, H., & Duchaine, B. (2018). Developmental prosopagnosics have widespread selectivity reductions across category-selective visual cortex. *Proceedings of the National Academy of Sciences*, *115*(28), E6418–E6427. https://doi.org/10.1073/pnas.1802246115

Jonas, J., Brissart, H., Hossu, G., Colnat-Coulbois, S., Vignal, J.-P., Rossion, B., & Maillard, L. (2018). A face identity hallucination (palinopsia) generated by intracerebral stimulation of the face-selective right lateral fusiform cortex. *Cortex*, *99*, 296–310. https://doi.org/10.1016/j.cortex.2017.11.022

Jonas, J., Descoins, M., Koessler, L., Colnat-Coulbois, S., Sauvée, M., Guye, M., Vignal, J.-P., Vespignani, H., Rossion, B., & Maillard, L. (2012). Focal electrical intracerebral stimulation of a face-sensitive area causes transient prosopagnosia. *Neuroscience*, *222*, 281–288. https://doi.org/10.1016/j.neuroscience.2012.07.021

Jonas, J., & Rossion, B. (2021). Intracerebral electrical stimulation to understand the neural basis of human face identity recognition. *European Journal of Neuroscience*, *54*(1). https://doi.org/10.1111/ejn.15235

Jonas, J., Rossion, B., Brissart, H., Frismand, S., Jacques, C., Hossu, G., Colnat-Coulbois, S., Vespignani, H., Vignal, J.-P., & Maillard, L. (2015). Beyond the core face-processing network: Intracerebral stimulation of a face-selective area in the right anterior fusiform gyrus elicits transient prosopagnosia. *Cortex, The Whole Is Greater Than the Sum of the Parts*, *72*, 140–155. https://doi.org/10.1016/j.cortex.2015.05.026

Jonas, J., Rossion, B., Krieg, J., Koessler, L., Colnat-Coulbois, S., Vespignani, H., Jacques, C., Vignal, J.-P., Brissart, H., & Maillard, L. (2014). Intracerebral electrical stimulation of a face-selective area in the right inferior occipital cortex impairs individual face discrimination. *NeuroImage*, *99*, 487–497. https://doi.org/10.1016/j.neuroimage.2014.06.017

Jung, H., Amini, M., Hunt, B. J., Murphy, E. I., Sadil, P., Halchenko, Y. O., Petre, B., Miao, Z., Kragel, P. A., Han, X., Heilicher, M. O., Sun, M., Collins, O. G., Lindquist, M. A., & Wager, T. D. (2025). Spacetop: A multimodal fMRI dataset unifying naturalistic processes with a rich array of experimental tasks. *Scientific Data*, *12*(1), Article 1465. https://doi.org/10.1038/s41597-025-05154-x

Kanel, D., Vanes, L. D., Pecheva, D., Hadaya, L., Falconer, S., Counsell, S. J., Edwards, D. A., & Nosarti, C. (2021). Neonatal white matter microstructure and emotional development during the preschool years in children who were born very preterm. *eNeuro*, *8*(5), ENEURO.0546-20.2021. https://doi.org/10.1523/ENEURO.0546-20.2021

Keogh, R., & Pearson, J. (2018). The blind mind: No sensory visual imagery in aphantasia. *Cortex; a Journal Devoted to the Study of the Nervous System and Behavior*, *105*, 53–60. https://doi.org/10.1016/j.cortex.2017.10.012

Kerns, S., Mello, A., & Duchaine, B. (2025). Two cases of prosopometamorphopsia whose distortions are face-specific in daily life and in testing with 510 object categories. *Journal of Vision*, *25*(9). https://doi.org/10.1167/jov.25.9.2911

Kieseler, M.-L., Dickstein, A., Krafian, A., Li, C., & Duchaine, B. (2022). HEVA – A new basic visual processing test. *Journal of Vision*, *22*(14), 4109. https://doi.org/10.1167/jov.22.14.4109

Kieseler, M.-L., & Duchaine, B. (2023). Persistent prosopagnosia following COVID-19. *Cortex*, *162*, 56–64. https://doi.org/10.1016/j.cortex.2023.01.012

Kinnear, P. R. (2002). New Farnsworth-Munsell 100 hue test norms of normal observers for each year of age 5-22 and for age decades 30-70. *British Journal of Ophthalmology*, *86*(12), 1408–1411. https://doi.org/10.1136/bjo.86.12.1408

Lachmund, D. (1904). Ueber vereinzelt auftretende halluzinationen bei epileptikern. *Monatsschrift Für Psychiatrie Und Neurologie*, *15*(6), 434–444. https://doi.org/10.1159/000219292

Landis, T., Cummings, J. L., Christen, L., Bogen, J. E., & Imhof, H.-G. (1986). Are unilateral right posterior cerebral lesions sufficient to cause prosopagnosia? Clinical and radiological findings in Six additional patients. *Cortex*, *22*(2), 243–252. https://doi.org/10.1016/S0010-9452(86)80048-X

Ma, D. S., Correll, J., & Wittenbrink, B. (2015). The Chicago face database: A free stimulus set of faces and norming data. *Behavior Research Methods*, *47*(4), 1122–1135. https://doi.org/10.3758/s13428-014-0532-5

Marks, D. F. (1973). Visual imagery differences in the recall of pictures. *British Journal of Psychology*, *64*, 17–24. https://doi.org/10.1111/j.2044-8295.1973.tb01322.x

Marks, D. F. (1995). New directions for mental imagery research. *Journal of Mental Imagery*, *19*, 153–167.

Mello, A., & Duchaine, B. (2025). What do we know about people with developmental prosopagnosia? In K. Lander (Ed.), *From super recognisers to the face blind* (pp. 39–74). Oxford University Press.

Mello, A., Garside, D., Stehr, D., Bujarski, K., Conway, B., & Duchaine, B. (2024). Color robustly affects the intensity of facial distortions in two cases of prosopometamorphopsia. *Journal of Vision*, *24*(10), 659. https://doi.org/10.1167/jov.24.10.659

Mello, A., Kodiweera, C., Stehr, D., Bujarski, K., & Duchaine, B. (2025). Visual perceptual distortions reveal an object-centered reference frame for faces and a stimulus-centered reference frame for hands. *Journal of Vision*, *25*(9). https://doi.org/10.1167/jov.25.9.2804

Mello, A., Stehr, D., Bujarski, K., & Duchaine, B. (2024). Visualising facial distortions in prosopometamorphopsia. *Lancet (London, England)*, *403*(10432), 1176. https://doi.org/10.1016/S0140-6736(24)00136-3

Mori, S., Oishi, K., Jiang, H., Jiang, L., Li, X., Akhter, K., Hua, K., Faria, A. V., Mahmood, A., Woods, R., Toga, A. W., Pike, G. B., Neto, P. R., Evans, A., Zhang, J., Huang, H., Miller, M. I., van Zijl, P., & Mazziotta, J. (2008). Stereotaxic white matter atlas based on diffusion tensor imaging in an ICBM template. *NeuroImage*, *40*(2), 570–582. https://doi.org/10.1016/j.neuroimage.2007.12.035

Moscovitch, M., Winocur, G., & Behrmann, M. (1997). What is special about face recognition? Nineteen experiments on a person with visual object agnosia and dyslexia but normal face recognition. *Journal of Cognitive Neuroscience*, *9*(5), 555–604. https://direct.mit.edu/jocn/article-abstract/9/5/555/3383

Motomura, K., Fujii, M., Maesawa, S., Kuramitsu, S., Natsume, A., & Wakabayashi, T. (2014). Association of dorsal inferior frontooccipital fasciculus fibers in the deep parietal lobe with both Reading and writing processes: A brain mapping

study: Case report. *Journal of Neurosurgery*, *121*(1), 142–148. https://doi.org/10.3171/2014.2.JNS131234

Mouka, V., Drougia, A., Xydis, V. G., Astrakas, L. G., Zikou, A. K., Kosta, P., Andronikou, S., & Argyropoulou, M. I. (2019). Functional and structural connectivity of the brain in very preterm babies: Relationship with gestational age and body and brain growth. *Pediatric Radiology*, *49*(8), 1078–1084. https://doi.org/10.1007/s00247-019-04412-6

Mullen, K. M., Vohr, B. R., Katz, K. H., Schneider, K. C., Lacadie, C., Hampson, M., Makuch, R. W., Reiss, A. L., Constable, R. T., & Ment, L. R. (2011). Preterm birth results in alterations in neural connectivity at age 16 years. *NeuroImage*, *54*(4), 2563–2570. https://doi.org/10.1016/j.neuroimage.2010.11.019

Mundel, T., Milton, J. G., Dimitrov, A., Wilson, H. W., Pelizzari, C., Uftring, S., Torres, I., Erickson, R. K., Spire, J.-P., & Towle, V. L. (2003). Transient inability to distinguish between faces: Electrophysiologic studies. *Journal of Clinical Neurophysiology*, *20*(2), 102–110. https://journals.lww.com/clinicalneurophys/abstract/2003/04000/transient_inability_to_distinguish_between_faces_.3.aspx

Norman-Haignere, S., Kanwisher, N., & McDermott, J. H. (2013). Cortical pitch regions in humans respond primarily to resolved harmonics and are located in specific tonotopic regions of anterior auditory cortex. *The Journal of Neuroscience: The Official Journal of the Society for Neuroscience*, *33*(50), 19451–19469. https://doi.org/10.1523/JNEUROSCI.2880-13.2013

Oishi, K., Zilles, K., Amunts, K., Faria, A., Jiang, H., Li, X., Akhter, K., Hua, K., Woods, R., Toga, A. W., Pike, G. B., Rosa-Neto, P., Evans, A., Zhang, J., Huang, H., Miller, M. I., van Zijl, P. C. M., Mazziotta, J., & Mori, S. (2008). Human brain white matter atlas: Identification and assignment of common anatomical structures in superficial white matter. *NeuroImage*, *43*(3), 447–457. https://doi.org/10.1016/j.neuroimage.2008.07.009

Parvizi, J., Jacques, C., Foster, B. L., Withoft, N., Rangarajan, V., Weiner, K. S., & Grill-Spector, K. (2012). Electrical stimulation of human fusiform face-selective regions distorts face perception. *Journal of Neuroscience*, *32*(43), 14915–14920. https://doi.org/10.1523/JNEUROSCI.2609-12.2012

Peterson, R. L., & Pennington, B. F. (2015). Developmental dyslexia. *Annual Review of Clinical Psychology*, *11*, 283–307. https://doi.org/10.1146/annurev-clinpsy-032814-112842

Philippi, C. L., Mehta, S., Grabowski, T., Adolphs, R., & Rudrauf, D. (2009). Damage to association fiber tracts impairs recognition of the facial expression of emotion. *Journal of Neuroscience*, *29*(48), 15089–15099. https://doi.org/10.1523/JNEUROSCI.0796-09.2009

Pitcher, D., Dilks, D. D., Saxe, R. R., Triantafyllou, C., & Kanwisher, N. (2011). Differential selectivity for dynamic versus static information in face-selective cortical regions. *NeuroImage*, *56*(4), 2356–2363. https://doi.org/10.1016/j.neuroimage.2011.03.067

Pitcher, D., Walsh, V., & Duchaine, B. (2011). The role of the occipital face area in the cortical face perception network. *Experimental Brain Research*, *209*(*4*), 481–493. https://doi.org/10.1007/s00221-011-2579-1

Pounder, Z., Stantić, M., Reeder, R., Catmur, C., & Bird, G. (2026). Individuals with aphantasia show independent impairments in face perception and face memory, but not face matching. *Cortex*, *202*, 157–164. https://doi.org/10.1016/j.cortex.2026.06.002

Puce, A., Allison, T., & McCarthy, G. (1999). Electrophysiological studies of human face perception. III: Effects of top-down processing on face-specific potentials. *Cerebral Cortex*, *9*(5), 445–458. https://doi.org/10.1093/cercor/9.5.445

Rangarajan, V., Hermes, D., Foster, B. L., Weiner, K. S., Jacques, C., Grill-Spector, K., & Parvizi, J. (2014). Electrical stimulation of the left and right human fusiform gyrus causes different effects in conscious face perception. *Journal of Neuroscience*, *34*(38), 12828–12836. https://doi.org/10.1523/JNEUROSCI.0527-14.2014

Reynolds, R. C., Taylor, P. A., & Glen, D. R. (2023). Quality control practices in FMRI analysis: Philosophy, methods and examples using AFNI. *Frontiers in Neuroscience*, *16*, 1073800. https://doi.org/10.3389/fnins.2022.1073800

Rezlescu, C., Chapman, A., Susilo, T., & Caramazza, A. (2024). *Large inversion effects are not specific to faces and do not vary with object expertise*. https://doi.org/10.1167/17.10.250.

Rezlescu, C., Danaila, I., Miron, A., & Amariei, C. (2020). Chapter 13 - more time for science: Using testable to create and share behavioral experiments faster, recruit better participants, and engage students in hands-on research. In B. L. Parkin (Ed.), *Progress in brain research* (pp. 243–262). Elsevier.

Rivest, J., Moscovitch, M., & Black, S. (2009). A comparative case study of face recognition: The contribution of configural and part-based recognition systems, and their interaction. *Neuropsychologia*, *47*(13), 2798–2811. https://www.sciencedirect.com/science/article/pii/S0028393209002553

Rosenke, M., van Hoof, R., van den Hurk, J., Grill-Spector, K., & Goebel, R. (2021). A probabilistic functional atlas of human occipito-temporal visual Cortex. *Cerebral Cortex*, *31*(1), 603–619. https://doi.org/10.1093/cercor/bhaa246

Schalk, G., Kapeller, C., Guger, C., Ogawa, H., Hiroshima, S., Lafer-Sousa, R., Saygin, Z. M., Kamada, K., & Kanwisher, N. (2017). Facephenes and rainbows: Causal evidence for functional and anatomical specificity of face and color processing in the human brain. *Proceedings of the National Academy of Sciences*, *114*(46), 12285–12290. https://doi.org/10.1073/pnas.1713447114

Scherf, K. S., Behrmann, M., Humphreys, K., & Luna, B. (2007). Visual category-selectivity for faces, places and objects emerges along different developmental trajectories. *Developmental Science*, *10*(4), F15–F30. https://doi.org/10.1111/j.1467-7687.2007.00595.x

Schrouff, J., Raccah, O., Baek, S., Rangarajan, V., Salehi, S., Mourão-Miranda, J., Helili, Z., Daitch, A. L., & Parvizi, J. (2020). Fast temporal dynamics and causal relevance of face processing in the human temporal cortex. *Nature Communications*, *11*(1), Article 656. https://doi.org/10.1038/s41467-020-14432-8

Sigurdardottir, H. M., Arnardottir, A., & Halldorsdottir, E. T. (2021). Faces and words are both associated and dissociated as evidenced by visual problems in dyslexia. *Scientific Reports*, *11*(1), Article 23000. https://doi.org/10.1038/s41598-021-02440-7

Stehr, D. A., Zhang, Y., Patgiri, A., Kidder, A., Kay, K., & Duchaine, B. (2025). Developmental prosopagnosics have normal spatial integration in posterior ventral face-selective regions. *eLife*. https://doi.org/10.7554/eLife.108657.1

Stigliani, A., Weiner, K. S., & Grill-Spector, K. (2015). Temporal processing capacity in high-level visual cortex Is domain specific. *Journal of Neuroscience*, *35*(36), 12412–12424. https://doi.org/10.1523/JNEUROSCI.4822-14.2015

Sugahara, Y., Iizuka, C., Doi, K., Matsuzaki, K., & Nagaoka, M. (2022). False recognition/misidentification of unfamiliar person after cerebral infarction: A case report. *Cortex*, *147*, 185–193. https://doi.org/10.1016/j.cortex.2021.12.005

Taddei, M., Tettamanti, M., Zanoni, A., Cappa, S., & Battaglia, M. (2012). Brain white matter organisation in adolescence is related to childhood cerebral responses to facial expressions and harm avoidance. *NeuroImage*, *61*(4), 1394–1401. https://doi.org/10.1016/j.neuroimage.2012.03.062

Tangen, J. M., Murphy, S. C., & Thompson, M. B. (2011). Flashed face distortion effect: Grotesque faces from relative spaces. *Perception*, *40*(5), 628–630. https://doi.org/10.1068/p6968

Thompson, P. (1980). Margaret thatcher: A new illusion. *Perception*, *9*(4), 483–484. https://doi.org/10.1068/p090483

Tsao, D. Y., & Livingstone, M. S. (2008). Mechanisms of face perception. *Annual Review of Neuroscience*, *31*, 411–437. https://doi.org/10.1146/annurev.neuro.30.051606.094238

Vollmer, B., Lundequist, A., Mårtensson, G., Nagy, Z., Lagercrantz, H., Smedler, A.-C., & Forssberg, H. (2017). Correlation between white matter microstructure and executive functions suggests early developmental influence on long fibre tracts in preterm born adolescents. *PLoS One*, *12*(6), e0178893. https://doi.org/10.1371/journal.pone.0178893

Warrington, E. K. (1984). Recognition memory test. *Western Psychological Services*.

Weiner, K. S., Golarai, G., Caspers, J., Chuapoco, M. R., Mohlberg, H., Zilles, K., Amunts, K., & Grill-Spector, K. (2014). The mid-fusiform sulcus: A landmark identifying both cytoarchitectonic and functional divisions of human ventral temporal cortex. *NeuroImage*, *84*, 453–465. https://doi.org/10.1016/j.neuroimage.2013.08.068

Wen, T., & Kung, C.-C. (2014). Using functional magnetic resonance imaging to explore the flashed face distortion effect. *Journal of Vision*, *14*(12), 29. https://doi.org/10.1167/14.12.29

Young, J. M., Vandewouw, M. M., Morgan, B. R., Smith, M. L., Sled, J. G., & Taylor, M. J. (2018). Altered white matter development in children born very preterm. *Brain Structure and Function*, *223*(5), 2129–2141. https://doi.org/10.1007/s00429-018-1614-4